SLAC-PUB-674
September 1969
(TH) and (EXP)

# HIGH ENERGY ELECTROPRODUCTION*

Frederick J. Gilman
Stanford Linear Accelerator Center, Stanford University, Stanford, California

Invited talk presented at the
1969 International Symposium on Electron and Photon Interactions at High Energies
Liverpool, England
September 14 to 20, 1969

*Work supported by the U.S. Atomic Energy Commission.

## 1. Introduction

A simple way to establish the compositeness of a sub-microscopic object is to break up the object and look for the constituents in the debris. A somewhat refined way of doing this is to scatter a known particle with known interactions on the object of interest and observe the results of such scatterings. In particular, if we were to systematically scatter electrons of various energies on the object and just observe the energy and angle of the scattered electrons, we can determine the instantaneous charge distribution within the object and hence "observe" the constituents without actually looking directly for them in the debris.

As an example, we have in figure 1 the results of scattering 400 keV electrons off of Aluminum and Gold atoms at various angles.[1] The "channel number" is directly proportional to the final electron energy. Looking at the right side of the graphs we see the elastic peak (which also includes excitations to the discrete atomic levels) and then, as we go to the left (lower final electron energies) we have a steep rise and plateau corresponding to electrons and photons being knocked out of the atom. For laboratory angles less than $90^{o}$ (e.g., $40^{o}$ in figure 1) one can see a "quasi-elastic peak" which is due to the incident electrons scattering off the constituent electrons of the atom.

Similar studies have been conducted on nuclei. In figure 2 we have the spectum of final electron energies[2] arising from scattering electrons on $C^{12}$. Again one sees the elastic peak to the right, to the left of that the excitation of discrete levels, and finally a large quasi-elastic peak due to electron scattering off of the constituent nucleons within the nucleus.

In both these cases while things look very good qualitatively, the detailed quantitative analysis of the electron scattering data is not so simple. In the atomic case, even though we know what the constituents are and the forces between them, no one has yet been able to make a satisfactory calculation of the spectra shown in figure 1 (in particular, the large magnitude of the large angle data is unexplained). In the nuclear physics case, we think we know what the constituents are, if not the forces, and fairly rough calculations based on a Fermi gas model fit the quasi-elastic peak rather well.[3)]

Now for the nucleon, the main subject of this talk, we know neither what the constituents are nor what the forces are, even though I would guess that most high energy theorists do believe that the nucleon is composite in one sense or another. Our lack of understanding of strong interaction dynamics will of course prevent us from doing much in the way of quantitative predictions, especially since, as we have just seen, even in cases where we know what is going on it is sometimes difficult to do detailed calculations. At least to start with our plan of attack for extracting information on the composite structure of the nucleon through electron scattering should then try and use either aspects of the data which are independent of the strong interaction dynamics (such as the rough position and shape of a quasi-elastic peak), or which involve only general aspects of strong interaction processes which are fairly well understood (such as the high energy behavior of total cross sections). Let us then turn to the experimental data to see what it tells us.

## 2. Kinematics and the Experimental Data

We are interested here in exploring the data and its consequences for the process shown in figure 3: an electron of energy E scatters off a nucleon (of four-momentum P) at an angle $\theta$ and with final energy E', producing the final state n by means of the exchange of a photon (of four-momentum q). Since we know the interaction at the electron-photon vertex and the photon propagator, we may take these factors out of the data and study what is happening at the lower vertex. Here, if we don't observe the details of the final hadronic state (i.e., if we average over initial proton spin and sum over all final hadronic states) then everything must be a function of just the two Lorentz scalar variables[4]

$$q^2 = 4EE' \sin^2(\theta/2) \tag{1}$$

and

$$\nu = q_o = -q\cdot P/M_N = E - E' , \tag{2}$$

the photon (mass)$^2$ and energy in the laboratory. The invariant mass, W of the final hadronic state is related to $\nu$ and $q^2$ by

$$\nu = \frac{W^2 - M_N^2 + q^2}{2M_N} . \tag{3}$$

From a theoretical point of view we are measuring the quantity (an average over nucleon spin is understood)

$$W_{\mu\nu} = \frac{1}{4\pi\alpha}\sum_n < P| J_\mu^{(em)}(0)|n><n| J_\nu^{(em)}(0)| P> (2\pi)^3 \delta^{(4)}(p_n - P - q) \qquad (4)$$

which, by Lorentz and gauge invariance can be written as[5)]

$$W_{\mu\nu} = W_1\left(\nu, q^2\right)\left(\delta_{\mu\nu} - \frac{q_\mu q_\nu}{q^2}\right) + W_2(\nu, q^2)\left(P_\mu - \frac{P\cdot q q_\mu}{q^2}\right)\left(P_\nu - \frac{P\cdot q q_\nu}{q^2}\right)\Big/ M^2{}_N. \qquad (5)$$

The quantity $W_{\mu\nu}$ is just $(1/4\pi^2\alpha)$ times the imaginary part of the virtual forward Compton scattering amplitude for photons of mass$^2 = -q^2$. In terms of $W_1$ and $W_2$ the experimentally measured double differential cross-section is

$$\frac{d^2\sigma}{d\Omega' dE'} = \frac{4\alpha^2 (E')^2}{q^4}\left[2W_1\left(\nu, q^2\right)\sin^2(\theta/2) + W_2\left(\nu, q^2\right)\cos^2(\theta/2)\right]. \qquad (6)$$

Roughly, at small angles one measures $W_2$; at large angles $W_1$.

One other set of kinematic quantities has come into common use: these are the transverse and longitudinal cross-sections $\sigma_T$ and $\sigma_S$ due to Hand.[6)] In terms of these

$$\frac{d^2\sigma}{d\Omega' dE'} = \frac{\alpha}{4\pi^2}\,\frac{K}{q^2}\,\frac{E'}{E}\left(\frac{2}{1-\epsilon}\right)(\sigma_T + \epsilon\sigma_S) \qquad (7)$$

where

$$K = \nu - q^2/2M_N$$

and

$$\epsilon = \frac{1}{1 + 2(1 + \nu^2/q^2)\tan^2 \theta/2},$$

so that $0 \leq \epsilon \leq 1$. On comparison with Eq. (6) we have the relations[7]

$$W_1(\nu, q^2) = \frac{K}{4\pi^2 \alpha} \sigma_T(\nu, q^2) \tag{8}$$

$$W_2(\nu, q^2) = \frac{K}{4\pi^2 \alpha} \frac{q^2}{q^2 + \nu^2} \left(\sigma_T(\nu, q^2) + \sigma_S(\nu, q^2)\right) :$$

At $q^2 = 0$, $\sigma_T(\nu, q^2) \rightarrow \sigma_T(\nu, 0)$, the total photoabsorption cross section on protons of photons with energy $\nu$; this has been measured from threshold to almost 20 GeV in a series of beautiful experiments[8] in the past year (see figure 4). The quantity $\sigma_S(\nu, q^2)$ must vanish at $q^2 = 0$ because of kinematic constraints.

The results of experiments are then to be summarized in terms of the amplitudes $W_1$ and $W_2$ (or alternately $\sigma_T$ and $\sigma_S$) as they depend on $\nu$ and $q^2$. A kinematic map of this new land which we want to explore, the $\nu - q^2$ plane, is shown in figure 5. The lines at fixed W correspond to fixed hadronic missing mass. No measurement can be made to the left of the line $W = 0.94$ GeV/$c^2 = M_N$, which corresponds to elastic scattering;

measurements along this line correspond to the usual measurements of the nucleon form factors, some of which are now known out to $q^2 = 25$ GeV$^2$. The line $q^2 = 0$ corresponds to the measurement of the total photoabsorption cross section, which is now known out to almost $\nu = 20$ GeV. It is then the large region bounded by these two lines which we now wish to explore. The lines in figure 5 at fixed values of $2 M_N \nu / q^2$, as we shall shortly see, are very useful in discussing the shape of the data.

In figure 6 we see the lines along which experimental data was taken in the recent SLAC experiments. The results of the $6^\circ$ and $10^\circ$ measurements[9] are reported to this conference, while the larger angle data exists in preliminary form[10]. Where two fixed $\theta$ lines cross at a given value of $\nu$ and $q^2$, one can separate $W_1$ and $W_2$ or $\sigma_T$ and $\sigma_S$, exactly as one can separate $G_M^2$ and $G_E^2$ for the case of elastic scattering.

A typical result of such a series of measurements at a fixed angle and incident energy is shown in figure 7a for $E = 10.0$ GeV and $\theta = 6^\circ$. Of little interest to theorists, but of much trouble for experimentalists, is the fact that such a set of data must be radiatively corrected to give the spectrum shown in figure 7b. While a nuisance, the problem of doing the radiative corrections is well understood and now seems to be well under control. In figure 8 we see three other spectra at increasing energies and angles (and therefore increasing $q^2$). From the collected set of such spectra the following general features have emerged:

(1) As $q^2$ increases the prominent resonance bumps rapidly go away, more or less like the nucleon form factor squared.

(2) What is left is a smooth spectrum which is large, i.e., at fixed $q^2$, on integrating the spectrum over $\nu$ we get a result which is the

same order of magnitude as the Mott cross section due to scattering of electrons by a point proton.

(3) For a fixed missing mass $W \geq 2$BeV, the cross section falls off rather slowly in $q^2$, roughly like $1/q^2$ rather than the $1/q^8$ of the nucleon form factors squared.

(4) From the preliminary SLAC large angle data[11] and from the results of Albrecht et al.,[11] who have combined the SLAC small angle and the DESY large angle data we now have the first separations of $\sigma_S$ and $\sigma_T$ (or $W_1$ and $W_2$). Very conservatively, it appears that in the region out to $\nu = 10$ GeV and out to $q^2 = 5$ GeV$^2$ that $R = \sigma_S/\sigma_T < 1$. If anything, from the DESY analysis the ratio R seems to go down somewhat between $q^2 = .8$ GeV$^2$ and $q^2 = 2.0$ GeV$^2$, where it is consistent with zero.[12] In general, for $q^2 \geq 1.5$ GeV$^2$ it appears $R < 0.5$, is consistent within the present errors with zero, and does not depend strongly on any variable (neither $\nu$ nor $q^2$ nor $\nu/q^2$).

## 3. Point-like Constituents - The Parton Model

The large magnitude of the inelastic cross sections leads one to consider models where the proton is composed of point-like constituents. The key means of implementing such a model is to view the proton in the infinite momentum frame of reference where the proton is Lorentz contracted into a thin pancake and the motion of the constituents is slowed down to a standstill by time-dilation. In such a frame, and with $q^2$ large (compared to $M_N^2$ or any transverse moment squared), the electron can be viewed as scattering instantaneously and incoherently off the individual, point-like constituents.[13), 14)]

We thus can treat the constituents as "free" during the interaction and thereby hopefully avoid, at least partly, our ignorance of strong interaction dynamics.

In somewhat more detailed form, the assumptions[15] are (see figure 9)

(1) The nucleon consists of a number (N) of point-like constituents (partons) which can be treated as free particles in the infinite momentum frame.

(2) The partons have negligible transverse momenta (compared to $\sqrt{q^2}$) and, as $P \to \infty$, the i'th parton has (neglecting masses and transverse momenta) a fraction $x_i$ of the total momentum of the proton

$$p_i^\mu = x_i P^\mu. \tag{9}$$

(3) In the infinite momentum frame the electron scatters instantaneously off the point-like parton leaving it with the same mass and charge.

A small calculation then shows that the contribution of a single parton (with a fraction x of the longitudinal momentum) to $W_2(\nu, q^2)$ is:

$$\begin{aligned} W_2^{(i)}(\nu, q^2) &= Q_i^2 \delta(\nu - q^2/2M_N x) \\ &= \frac{Q_i^2 x}{\nu} \delta(x - q^2/2M_N \nu). \end{aligned} \tag{10}$$

Thus $\nu W_2$ for a distribution of partons is given by

$$\nu W_2(\nu, q^2) = \nu \sum_N P(N) \Big(\sum_{i=1}^{N} Q_i^2\Big)_N \int_0^1 dx f_N(x)\, \delta(\nu - q^2/2M_N x)$$

$$= \sum_N P(N) \Big(\sum_{i=1} Q_i^2\Big)_N x f_N(x) \Big|_{x = q^2/2M_N\nu} \tag{11}$$

$$= F(x = q^2/2M_N\nu),$$

where P(N) is the probability of N partons occurring, $\Big(\sum_{i=1}^{N} Q_i^2\Big)_N$ is the sum of the squares of the charges of the N partons, and $f_N(x)$ gives the distribution of longitudinal momentum of the partons. The quantity $\nu W_2(\nu, q^2) = F(x)$ is then predicted to be a function of just one variable, $x = q^2/2M\nu$ for large $q^2$ and $\nu$, and the shape of $F(x)/x$ gives a weighted average of $f_N(x)$, the distribution of longitudinal momenta among the partons. Thus $\nu W_2(\nu, q^2)$ should be a so-called "universal function" of $q^2/2M\nu$, something originally predicted for $\nu W_2$ and $W_1$ as $\nu$ and $q^2 \to \infty$ using more formal means by Bjorken.[16] This behavior of $\nu W_2$ can also be seen from the fact that we have put no internal mass scale in our calculations of $\nu W_2$, so it should be "scale invariant," i.e., a function of only the ratio $2q \cdot P/q^2 = 2M_N\nu/q^2$ of dot products of the external momenta.

Furthermore by normalization,

$$\int_0^1 f_N(x_i) dx_i = 1, \tag{12}$$

and, assuming a symmetric distribution of momenta among the partons,

$$\int_0^1 x_i f_N(x_i) dx_i = 1/N, \tag{13}$$

so that we have the sum rules[17]

$$\int_0^\infty d\nu\, W_2(\nu, q^2) = \int_0^1 \frac{dx}{x} F(x) = \sum_N P(N) \sum_{i=1}^N Q_i^2 \tag{14}$$

and

$$\frac{q^2}{2M_N} \int_0^\infty \frac{d\nu}{\nu} W_2(\nu, q^2) = \int_0^1 dx F(x) = \sum_N P(N) \left( \frac{\sum_{i=1}^N Q_i^2}{N} \right), \tag{15}$$

relating moments of the data to the sum of the squares of the charges of the partons and the average charge squared of the partons.

The obvious way to test if $\nu W_2$ is only a function of $2M_N\nu/q^2$ is to plot each of the data points versus $\omega = 2M_N\nu/q^2$ and see if one gets a single "universal curve". In figures 10 and 11 we have such plots[18] for $\nu W_2$ taken from the SLAC $6^\circ$ and $10^\circ$ data, respectively. Since these plots were made before it was established that $R = \sigma_S/\sigma_T$ is small, the two extreme cases $R = \infty$ (figures 10b and 11a) and $R = 0$ (figures 10c and 11b) were used for each data point to calculate $\nu W_2$ from the measured values of $d^2\sigma/d\Omega' dE'$. Clearly, for $R = 0$ one has a very striking "universal curve" for both the $6^\circ$ and $10^\circ$ data (figure 10a shows the results of the $E = 7.0$ GeV, $\theta = 6^\circ$ run separately

since it contains points at very small values of $q^2$ where there is no chance of having a "universal curve").

This is seen again in figure 12 where both the $6^o$ and $10^o$ data (taking only points with $q^2 \geq 1.0$ GeV$^2$ and assuming R = 0) are plotted on the same graph versus $x = q^2/2M_N\nu$, which makes it easier to "see" the point at $\nu = \infty$.

Finally in figures 13 and 14 we have $\nu W_2$ and $W_1$ plotted versus $2M_N\nu/q^2$ on a linear scale (assuming R = 0). Starting at the right hand side of the graphs and going to the left, the $q^2$ values of the plotted points are 0.5, 0.7, 0.4; 0.75, 1.0; 1.6, 1.4, 1.2, 1.0, 0.6; and 1.3, 2.0, 1.7 and 1.0 GeV$^2$ respectively. Thus points with values of $q^2$ differing by more than a factor of two consistently lie on the same universal curve if R = 0. In addition:

(1) If we assume, for example, $R \geq 1$ for all the $6^o$ and $10^o$ data points, then we get a great scatter of the data when plotted versus $\nu/q^2$, i.e., there is no universal curve for the values of $q^2$ reached in the $6^o$ and $10^o$ data unless $\sigma_S/\sigma_T$ is small.

(2) If R = 0, then $\nu W_2$ reaches a peak value at $\omega = 2M_N\nu/q^2 \approx 5$ and then decreases at larger values of $\omega$. This fall off at large $\omega$ still appears to be true if we only take points with $q^2 \geq 1$ GeV$^2$. Note however that we only have a separation of $\sigma_S$ and $\sigma_T$ at relatively low values of $\nu/q^2$, and the "universal curve" could be much flatter[19] if $R \approx 1$ for some of the points at small values of $q^2$ and large values of $\nu/q^2$. (See also the discussion in the next section.)

(3) The values of the integrals $\int_{0.05}^{1} F(x)dx$ and $\int_{0.05}^{1}(F(x)/x)dx$ are $\approx$ 0.17 and 0.7, respectively, for the data shown in figure 12 (again assuming R = 0). While almost any reasonable extrapolation of the data to

$x = 0$ gives $\int_0^1 F(x)dx \approx 0.18$, the integral $\int_0^1 (F(x)/x)dx$ diverges logarithmically if $F(0) \neq 0$ and its value is therefore very sensitive to the lower limit of the integral.

Putting details aside, let me emphasize again that the most remarkable feature of all this is the "universal" or "scale-invariant" character of the data. Even for very non-asymptotic data points with $0.5\ \text{GeV}^2 \leq q^2 \leq 1.0\ \text{GeV}^2$ one already finds good agreement with a "universal curve"; this is better than we have any right to expect theoretically for such small values of $q^2$.

To illustrate what happens when one takes the parton model very seriously in a quantitative sense, I have chosen two extreme cases. First, let us say the proton is composed of three quarks with a symmetric, phase space distribution of momenta. Then we have

$$F(x) = \nu W_2(\nu, q^2) = x f_3(x) = 2x(1-x), \tag{16}$$

which gives $\int_0^1 F(x)dx = \sum_{i=1}^{3} Q_i^2/3 = \frac{1}{3}(\frac{1}{9} + \frac{4}{9} + \frac{4}{9}) = \frac{1}{3}$ and has a "quasi-elastic peak" at $x = 1/2$; it is clearly too big to fit the data (see figure 15). The second model is the opposite extreme: an infinite sea of quark-antiquark pairs with average $(\text{charge})^2 = \frac{1}{3}(\frac{1}{9} + \frac{1}{9} + \frac{4}{9}) = \frac{2}{9} = \int_0^1 F(x)dx$. Note that[20] any SU(3) triplet has charges Z, Z, and Z + 1, so that the average charge squared is $Z^2 + \frac{2}{3}Z + \frac{1}{3} \geq \frac{2}{9}$, with the minimum for $Z = -\frac{1}{3}$, which is the usual quark model. Therefore $\int_0^1 F(x)dx \geq \frac{2}{9}$ for a sea of SU(3) triplet-antitriplet pairs with a symmetric momentum distribution[21]. The experimental value of $\int_0^1 F(x)dx$ appears to be temptingly close to $\frac{2}{9} \approx 0.22$. Now

if we again assume a phase space distribution of momenta, $P(N) = 1/N(N-1)$ for $N = 2,4,6,\ldots$, then we get $F(x) = (2/9\ell n 2)/(2-x)$ which also does not fit the data well as it stands (see figure 15). The important point to realize here though is that with any finite number of constituents one gets a "quasi-elastic peak" and $F(0) = 0$; only with an infinite number of constituents ($P(N) \sim 1/N^2$) does one obtain $F(0) \neq 0$ and therefore $\nu W_2 \to$ const. $\neq 0$ as $\nu \to \infty$.

In the second model, by changing the momentum distribution and/or by starting with $N = 3$ or $N = 4$ one can obtain a much better fit to the data; in particular the latter change will make $F(1) = 0$. However, I leave it to the audience to read the rules of the game in the paper of Bjorken and Paschos[15] and then to make their own fit to the data; perhaps with a little bit of $q\bar{q}$ sea, a touch of $q\bar{q}q\bar{q}$, a pinch of three quarks, etc., you too can fit the data.

4. Diffraction Models

Rather than avoiding strong interaction dynamics, another theoretical path is to use to good advantage our knowledge of certain general features of purely hadronic high energy scattering amplitudes[22]. Instead of emphasizing $\nu W_2$ and $W_1$, we note that for large $\nu$ and fixed $q^2$,

$$\begin{aligned} \nu W_2 &\propto q^2(\sigma_T + \sigma_S) \\ W_1 &\propto \nu\sigma_T , \end{aligned} \tag{17}$$

and focus attention on the total cross sections $\sigma_T$ and $\sigma_S$. It appears that hadronic total cross sections are composed of two parts: first, the contribution of "ordinary" t-channel Regge poles (like $\rho, A_2, P', \ldots$) giving contributions to total cross sections which go to zero as $\nu \to \infty$, and which are related

through finite energy sum rules to the resonances at low energy; and second, the Pomeron or diffraction scattering, which gives constant total cross sections as $\nu \to \infty$ and is related to "background" at low energies[23].

Now if we look at the electron scattering data we see that the prominent resonances are rapidly going away as $q^2$ increases, and therefore, if we believe the above connection, so must be the "ordinary" Regge trajectories. This leaves us with the Pomeron as $q^2$ gets large, so that we expect $\sigma_T$ and $\sigma_S$ for large $\nu$ to become more and more flat as $q^2$ increases. At any fixed value of $q^2$, Eq. (17) shows that $\nu W_2$ should also become more and more flat[24], and, for each value of $q^2$, go to a non-zero constant value as $\nu \to \infty$.

In figures 16, 17, and 18 we attempt to test this by plotting $\nu W_2$ from the $6^o$ and $10^o$ data as a function of $\nu$ at $q^2 = 0.75$, 1.0, and 2.0 GeV$^2$ for the two values of R, R = 0 and R = 0.5. At $q^2 = 0.75$ GeV$^2$, $\nu W_2$ appears to be falling as $\nu$ increases, even if R = 0.5, while at $q^2 = 2.0$ GeV$^2$, $\nu W_2$ appears to be flat as a function of energy if R = 0 and rising if R = 0.5. One must be very careful, however, in making such comparisons, because if we do have a "universal curve" the data point at $\nu = 14$ GeV, $q^2 = 2.0$ GeV$^2$ in figure 18 should really be compared with one at $\nu = 7$ GeV for $q^2 = 1.0$ GeV$^2$ and one at $\nu = 5$ GeV for $q^2 = 0.75$ GeV$^2$. If we do that we see that we would have expected $\nu W_2 \approx 0.30$ at $\nu = 14$ GeV and $q^2 = 2.0$ GeV$^2$, something which is quite consistent with the data shown in figure 18. Thus, while figures 16, 17 and 18 are at least consistent with $\nu W_2$ getting flatter as $q^2$ increases, the present data is also quite consistent with a fall-off in $\nu W_2$ at large $\nu/q^2$. Unfortunately, I do not think we can definitely choose between these two possibilities with the present experimental data.

An immediate testable prediction of the diffraction model for electroproduction is that $\nu W_2$ for the proton and neutron should be the same. In general, what is not predicted, at least at first, is the $q^2$ dependence of the total cross sections. In other words, "scale invariance" must be put in by hand if we want it. If we assume scale invariance, then the $q^2$ dependence comes out trivially; for if $\nu W_2(\nu,q^2)$ is actually a function of only $\nu/q^2$ and goes to a constant independent of $\nu$ as $\nu \to \infty$, then the constant must be independent of $q^2$ also[25]. A very interesting way of getting the scale invariance for such a Pomeron model is to associate the diffraction with the infinite sea of $q\bar{q}$ pairs in a parton model which we discussed previously[26]. A particularly intriguing feature of making such an association is that the magnitude of the cross section, which is essentially geometrical in the Pomeron model (roughly related to the geometrical size of the proton), is connected to the average charge squared of the quarks in the parton model!

A very specific type of diffraction model is obtained by using vector dominance[27]. In particular, Sakurai[28] has proposed a model where the $q^2$ dependence of the total cross sections is given by

$$\sigma_T(\nu,q^2) = \left(\frac{M_V^2}{M_V^2+q^2}\right)^2 \sigma_T(K,\ q^2=0)\ , \tag{18a}$$

and

$$R = \frac{\sigma_S(\nu,q^2)}{\sigma_T(\nu,q^2)} = \left(\frac{q^2}{M_V^2}\right)\left(\frac{K^2}{\nu^2}\right)\xi\,(K)\ , \tag{18b}$$

where $K = \nu - q^2/2M_N = (W^2 - M_N^2)/(2M_N)$ and $\xi\,(K)$ is the ratio of the vector meson - nucleon (presumably dominantly rho-nucleon) total cross sections

for vector mesons with polarization vectors respectively parallel and perpendicular (i.e., helicity 0 and helicity ± 1) to their direction of motion. Since we expect $\xi \approx 1$ at high energies, such a theory predicts very large values of $R = \sigma_S/\sigma_T$ at large values of $q^2$. Note that the factor of $q^2$ in the numerator of Eq. (18b) is essential to fit the slow fall-off of the $6^o$ and $10^o$ data with $q^2$ ($\sigma_T + \sigma_S \sim 1/q^2$). This is because $\sigma_T$ in Eq. (18a) falls off like $1/q^4$, so the extra factor of $q^2$ in Eq. (18b) is what assures that $\sigma_S$ falls off like $1/q^2$ and therefore that $\sigma_T + \sigma_S$ falls off like $1/q^2$, permitting a rough fit to the small angle data.

All this is of course very easy to confront with experiment, and the preliminary large angle data from SLAC show[11] that both R and $\sigma_T$ predicted by the vector dominance model are in disagreement with experiment. In particular, the data show that R is small and does not grow rapidly with $q^2$ as Eq. (18b) would say. Moreover, given a value of R one can calculate $\sigma_T$ and $\sigma_S$ separately, and one then finds that it is $\sigma_T$ which is falling slowly with $q^2$ (roughly like $1/q^2$) and is chiefly responsible for the character of the data, in disagreement with Eq. (18a). So the preliminary large angle data very definitely rules out the vector dominance model as an explanation of the data and one can only hope that nobody is too emotionally attached to such theories.

## 5. Field Theory Models

An instructive thing to do, especially if you are a theorist, is to consider what happens to various more familiar models or theories when they are considered in the new limit of fixed $\nu/q^2$ with $\nu$ and $q^2 \to \infty$. A particular

case is virtual photons interacting with nucleons in the field theory consisting of nucleons and pions with $\gamma_5$ coupling, which has been considered in great detail by Drell, Levy and Yan[29]. They must assume that there exists a region where $q^2$ and $2M_N\nu$ are larger than the transverse momenta of all the particles involved in the theory, but given this assumption, by considering all graphs in each order of perturbation theory they can derive a parton model and show that the structure functions $W_1$ and $\nu W_2$ should depend on $\nu/q^2$ only. The partons in this model are the pions and nucleon making up the proton. It turns out that the interacting partons, i.e., the free, point-like consistuents which interact with the electromagnetic current in each order of perturbation theory and to leading order in logarithms of $2M_N\nu/q^2$, are the bare nucleons making up the proton and not the pions in the pion cloud. The net result of all this is that one is left with a sum of ladder graphs with pions as rungs and nucleons as sides for the forward (virtual) Compton amplitude and hence for the structure functions $W_1$ and $\nu W_2$ at large values of $2M_N\nu/q^2$. As is well known, such sums of ladder diagrams yield Regge behavior. Here the value of the Regge spin, $\alpha(0)$, depends on the strong coupling constant and the transverse momentum cut-off. With reasonable values for these parameters one can obtain a fit to the large $\nu/q^2$ data points.

A somewhat related study was made by Abarbanel, Goldberger and Treiman[30] who first noted that the relevant variable which must be large in order to make Regge expansions, which is $\cos\theta_t$, turns out to be approximately proportional to $\nu/\sqrt{q^2}$ in the case of virtual forward Compton scattering. This quantity is already fairly large for many of the present SLAC data points, and for fixed $\nu/q^2$, $\nu/\sqrt{q^2} \to \infty$ as $\nu$ and $q^2 \to \infty$. Thus we would expect the Regge

representation to be a better and better description as we go to the limit where we expect scaling to hold. One, at first sight, worrisome aspect of this is that the forward amplitude for virtual Compton scattering will not scale, i.e. be a function of $\nu/q^2$, unless the Regge residue function, $\beta(q^2)$ is very "smart". This has been investigated by the above authors in a model consisting of a sum of ladder graphs made out of scalar particles and it is found that $\beta(q^2)$ is (or really, almost is) "smart" enough to give the right function of $q^2$ to make the whole amplitude scale[31].

A very different aspect of field theory has been emphasized by Cheng and Wu in connection with their recent monumental calculations of the high energy behavior of scattering amplitudes in quantum electrodynamics[32]. By summing all diagrams up through sixth order in Compton scattering they found expressions for the total cross section which go to constant values as the energy, $\nu$, goes to infinity. Other authors have since shown how to generalize their result of constant total cross sections to all orders by summing all the s-channel ladder diagrams with photon (i.e., vector meson) exchanges[33]. If they extend their results to $q^2 \neq 0$, then they find that[34] $\nu W_2$ and $q^2\sigma$ go to constants as $\nu \to \infty$, $q^2$ fixed, but they do not scale, and in fact contain terms like $\ell n(q^2/\lambda^2)$ where $\lambda^2$ is the vector meson mass. Thus for reasonable values of $\lambda^2$ one would have expected to see rather large violations of scaling in the SLAC data.

## 6. Related Processes and Implications

One of the very pleasant aspects of the subject of this talk is that it is not a dead-end, disconnected from the rest of physics, but has many

experimental and theoretical implications for other parts of high energy physics. In the remainder of this talk I would like to quickly discuss some of these related questions in both their experimental and theoretical aspects.

A. If one has a total cross section which is large and which falls-off slowly in $q^2$, then some of its parts should exhibit the same behavior. Clearly we expect some channels, e.g. single pion production, to fall rapidly as $q^2$ increases. But what about $\rho$ production? In models which explain the electroproduction data discussed above by means of diffraction or Pomeron exchange, one might well expect diffractive electroproduction of $\rho$ mesons to have a similar slow fall-off in $q^2$. An interesting possibility is that the angular distribution of $\rho$ production becomes broader as $q^2$ increases, resulting in a slowly falling integrated cross section for $\gamma + p \rightarrow \rho^0 + p$ even though the forward differential cross section is decreasing fairly rapidly as $q^2$ increases. In various parton or diffraction theories one can also make predictions about the percentage of strange particles produced, the charged to neutral ratio for $S = 0$ mesons produced, the longitudinal momentum distribution of the final mesons or baryons, etc.[35].

B. Bjorken and Paschos[15] have studied the process $\gamma + p \rightarrow \gamma +$ "anything", i.e. inelastic Compton scattering of photons from protons, within the parton model. They find that for inelastic scattering at large momentum transfers,

$$\left(\frac{d^2\sigma}{d\Omega' dE'}\right)_{\gamma p} = \frac{\nu^2}{kk'}\left(\frac{d^2\sigma}{d\Omega' dE'}\right)_{ep} \frac{\langle \sum_i Q_i^4 \rangle}{\langle \sum_i Q_i^2 \rangle}, \qquad (19)$$

which, if measurable, might permit one to tell fractional from integrally charged partons.

C. Electron-positron annihilation processes offer another place where the point-like behavior of constituents of the proton might manifest itself. In particular, the process $e^+ + e^- \rightarrow$ proton + "anything" (see figure 19) has structure functions $\overline{W}_1$ and $\overline{W}_2$ which are related by the substitution rule to the structure functions $W_1$ and $W_2$ in inelastic electron scattering:

$$\overline{W}_1(\nu,q^2) = -W_1(-\nu,q^2)$$

and (20)

$$\overline{W}_2(\nu,q^2) = -W_2(-\nu,q^2) .$$

Although diffraction models of inelastic electron scattering in general say little about such processes, within the parton model, and using the same assumptions as for inelastic electron scattering, Drell, Levy and Yan[29] have shown that $\overline{W}_1$ and $\overline{W}_2$ should also become universal functions of $2M\nu/q^2$ for large $q^2$ and $2M\nu$. This leads one to expect large, i.e. point-like, cross sections for $e^+ + e^- \rightarrow p$ + "anything" and a total cross section for this process which varies as $1/q^2$, just as do those for a point particle (e.g., $\sigma(e^+ + e^- \rightarrow \mu^+ + \mu^-) = (1/3)(4\pi\alpha^2)/q^2$).

D. Obviously, if we have a property of the matrix elements of the vector current, then one is inclined to look for similar properties of the matrix elements of the axial-vector current. This can be done in the case we are interested in by doing high energy neutrino and anti-neutrino inelastic scattering[36]. For such processes, not only do we have the structure functions $W_1^{(\pm)}$ and $W_2^{(\pm)}$ which now get contributions from both the vector and axial-vector currents, but also a structure function $W_3^{(\pm)}$ which arises from the interference

between the vector and axial-vector currents. We have for $\left(\frac{\nu}{\bar{\nu}}\right) + p \rightarrow \left(\frac{\ell}{\bar{\ell}}\right) +$ "anything" in an obvious notation:

$$\frac{d^2\sigma}{d\Omega' dE'} = \frac{G^2(E')^2}{2\pi^2} \left[ 2 \sin^2\left(\frac{\theta}{2}\right) W_1^{(\pm)}(\nu, q^2) + \cos^2\left(\frac{\theta}{2}\right) W_2^{(\pm)}(\nu, q^2) \right.$$
$$\left. \mp \frac{E+E'}{M_N} \sin^2\left(\frac{\theta}{2}\right) W_3^{(\pm)}(\nu, q^2) \right] . \tag{21}$$

In a parton model we again expect $W_1$, $\nu W_2$, and $\nu W_3$ to scale at large $\nu$ and $q^2$, i.e. to be functions of $\nu/q^2$, and that the total cross section for $\left(\frac{\nu}{\bar{\nu}}\right) + p \rightarrow \left(\frac{\ell}{\bar{\ell}}\right) +$ "anything" should, in the same limit, exhibit the point-like behavior

$$\sigma \approx \frac{G^2}{\pi} (M_N E) . \tag{22}$$

Further, in the parton model $W_3$ provides a measure of the number of baryon minus the number of anti-baryon partons. The present CERN heavy liquid bubble chamber results[37] are at least consistent with all this, particularly Eq. (22), but it is to early to draw strong detailed conclusions.

Note that in the diffraction model one expects $W_3$ and $W_i^{(-)} - W_i^{(+)}$ to go to zero for large values of $2M_N\nu/q^2$, since all these quantities are proportional to amplitudes arising from the exchange of negative charge conjugation trajectories (not the Pomeron) in a Regge analysis. The CERN heavy liquid bubble chamber results[37] are consistent in magnitude (and consistent with $W_3 = 0$) with the diffraction model, but I again think it is too early to draw any strong conclusions favoring one model or the other from the present data.

E. Must of what we have been saying can be rephrased in the language of current commutators. In fact, much effort has gone into studying how various limits of the virtual Compton amplitudes and/or sum rules over

the electroproduction data can be (at least formally) related to equal time commutators of the electromagnetic current with itself and with its time derivatives[38]. One can even take the point of view that certain integrals over moments of $W_1$ and $W_2$ define experimentally the value of certain commutators. One of course then hopes that these same commutators can also be calculated in some simple theoretical model and thereby compared with experiment.

A case in point is the commutator of a space component with its time derivative, which when calculated in a naive way is completely different for the quark model and for the algebra of fields. When the connection[39] is made back to experiment, this leads to the conclusion that for fixed $\nu/q^2$ and $q^2 \to \infty$, $\sigma_S/\sigma_T$ should vanish in the quark model while $\sigma_T/\sigma_S$ should vanish in the algebra of fields case. This is, of course, subject to direct experimental test and also agrees nicely with the parton model result that one expects $\sigma_S/\sigma_T$ to vanish in the same limit for spin-$\frac{1}{2}$ constituents while $\sigma_T/\sigma_S$ should vanish for spin-0 constituents; it therefore seems to put the parton results on a much firmer, more model independent basis. However, it was shown by Adler and Tung[40] and by Jackiw and Preparata[41], who explicitly constructed the Compton scattering amplitudes (whose imaginary part is the electroproduction structure functions) in perturbation theory for renormalizable field theories, that by taking the Bjorken limit one gets commutators for two space components of the current which do not agree with the naive ones. In other words, in perturbation theory the commutator defined by taking appropriate limits of the Compton amplitude does not agree with the naive one if we are dealing with two space components of the current (but does agree if at least one of the currents is the time component of a

current). It seems that we learn once more that the very singular parts (such as the equal time commutator of two space components of the vector current) of even "smooth" field theories are rather subtle and they can neither be dealt with in a naive manner, nor unambiguously subjected to experimental test.

F. Bjorken first noticed[42] that the sum rule

$$\int_0^\infty d\nu \left[ W_2^{(-)}(\nu,q^2) - W_2^{(+)}(\nu,q^2) \right] = 1 , \tag{23}$$

derived by Adler[43] for inelastic neutrino scattering from the commutator of two time components of the weak current, leads to the inequality for inelastic electron scattering

$$\int_{q^2/2M_N}^\infty d\nu \left| W_{2p}(\nu,q^2) + W_{2n}(\nu,q^2) \right| \geq \tfrac{1}{2} \tag{24}$$

because

$$W_2^{(-)}(\nu,q^2) - W_2^{(+)}(\nu,q^2) \leq W_2^{(-)}(\nu,q^2) + W_2^{(+)}(\nu,q^2) \leq 2\left[ W_{2p}(\nu,q^2) + W_{2n}(\nu,q^2) \right]. \tag{25}$$

From the present data $\int^{\nu_m} d\nu\, W_{2p}(\nu,q^2) \geq \frac{1}{4}$ for $\nu_m \approx 3q^2$ and $\int^{\nu_m} d\nu\, W_{2p}(\nu,q^2) \geq \frac{1}{2}$ for $\nu_m \approx 7q^2$. Unfortunately this may not tell us much since in using Eq. (25) to go from the equality, Eq. (23) (which corresponds to C = -1 in the t-channel so that we expect $W_2^{(-)}(\nu,q^2) - W_2^{(+)}(\nu,q^2) \to \nu^{\alpha_\rho(0)-2}$), to the inequality, Eq. (24) (which corresponds to C = +1 in the t-channel where we expect Pomeron exchange and $W_2 \to \nu^{\alpha_p(0)-2} = 1/\nu$), we go from a convergent

integral to a divergent one. Thus the Bjorken inequality can be satisfied by the diffraction contribution while the Adler equality itslef is violated[44].

Formally one can construct explicit solutions for the weak amplitudes which obey the Adler sum rule and do not conflict with the electroproduction data. For example, if we take $\nu/q^2 = 2.5$ as the top of the rise in $\nu W_{2p}(\nu,q^2)$ then at large $q^2$ the function

$$\nu W_2^{(-)}(\nu,q^2) - \nu W_2^{(+)}(\nu,q^2) = \tfrac{1}{2}\sqrt{\frac{2.5q^2}{\nu}}\ \Theta(\frac{\nu}{q^2} - 2.5) \qquad (26)$$

is scale invariant and has the properties:

(a) $$\nu W_2^{(-)}(\nu,q^2) - \nu W_2^{(+)}(\nu,q^2) \leq 2\nu W_{2p}(\nu,q^2) \leq 2\left[\nu W_{2p} + \nu W_{2n}\right]$$

(therefore consistent with experiment even if $W_{2n} = 0$), and

(b) $$\int_0^\infty d\nu \left[W_2^{(-)} - W_2^{(+)}\right](\nu,q^2) = 1\,,$$

and

(c) $$W_2^{(-)} - W_2^{(+)} \to \nu^{-3/2}$$

at fixed $q^2$ as $\nu \to \infty$ which corresponds to $\alpha_\rho(0) = \frac{1}{2}$. There has also been much activity during the year in constructing explicit virtual Compton scattering amplitudes of the Veneziano sort[45]. Although not of much "practical" use because of the narrow resonance assumption inherent in such models, they at least demonstrate the possibility of explicitly constructing amplitudes which obey the usual requirements of crossing, Regge behavior, current conservation, etc., as well as current algebra conditions and scaling. In any of

these cases though, one expects a sizable part[46] of $\nu W_{2p}$ to be non-diffractive and decreasing as $\nu \to \infty$.

G. From the work of Cottingham[47] there has been for some time now an expression for the neutron-proton mass difference in terms of differences of the electroproduction structure functions for the proton and neutron, integrated over $\nu$ and $q^2$. As is well known, the elastic contribution to the mass difference gives a result of the wrong sign. More recently, Harari[48] has shown that for the neutron-proton mass difference the dispersion relation for the virtual Compton amplitude $t_1(\nu,q^2)$ of Cottingham in general requires a subtraction, which at least explains our lack of success in calculating the mass difference using the contributions of low lying states to the dispersion integral.

In general one cannot determine such a real subtraction constant in a dispersion relation just from a knowledge of the imaginary part (given by the electroproduction data in this case). However, if one assumes that the high energy behavior of both the real and imaginary parts of the amplitude is that given by pure (and only one trajectory with $\alpha \geq 0$ in this case) Regge asymptotic behavior (presumably due to $A_2$ exchange in this case), then one can write sum rules which relate the subtraction to the Regge residue function and integrals over the electroproduction data. In the absence of neutron electroproduction data, one uses resonance saturation and finite energy sum rules to get the same thing. Recent analyses are rather discouraging — it still seems that even the correct sign does not come out of the calculations[49].

One can test the method of determining the subtraction constant in the case of the forward Compton amplitude for real photons. Here we already know the subtraction constant exactly — it is the Thomson limit, and the

imaginary part of the amplitude is given through the optical theorem by the recently measured total photoabsorption cross sections[8]. It has been suspected before that there may be a fixed pole at $\alpha = 0$ contributing to this amplitude, i.e., a real, non-zero constant term at high energies[50], but previous measurements of $\sigma_T(\gamma p)$ were not complete or accurate enough to show this conclusively. Such an extra real constant is just what could ruin our attempt to determine the subtraction constant, since it ruins the ratio of real to imaginary part predicted by pure Regge asymptotic behavior (which we have assumed in order to get the subtraction constant). From a re-evaluation[51] of the relevant sum rule and the dispersion relation using the total cross sections recently obtained from extrapolation of electron scattering, it appears that there is an extra (besides what Regge would predict), real, constant part in the Compton amplitude at high energies consistent in magnitude with the magnitude of the Thomson limit[52]. In other words, it appears that the method of determining the subtraction constant discussed above fails for the case of real Compton scattering. A similar[53] extra, real constant in the asymptotic virtual Compton amplitude could very well be responsible for the ruination of our attempts to calculate the neutron-proton mass difference.

## 7. Conclusion

Finally, what will the immediate future tell us. As the previous discussion indicates, we still have two quite different viewpoints which can be used to explain the present data. Within the parton model these might be roughly labelled as those involving dominantly a small number of interacting

partons (e.g., three quarks) and those involving dominantly an infinite number of partons (e.g., a sea of quark-antiquark pairs). Looked at from a t-channel point of view in virtual Compton scattering, the first possibility corresponds to "ordinary" exchanges (like P', $\rho$, $A_2$,...) being responsible for most of the cross section, while the second corresponds to Pomeron exchange. In the first case the Adler sum rule has a good chance of being right, while in the second case it is very likely wrong.

The most obvious experimental distinction between the two (besides neutrino experiments) can be made by observing if $\nu W_2$ goes down for large values of $\nu/q^2$ (favoring the first model) or is flat (favoring the second). To establish this we want data for large values of $\nu/q^2$ for the largest $q^2$ possible, so that we are in the scaling limit. In addition one needs a separation of $\sigma_T$ and $\sigma_S$ as far out in $\nu/q^2$ as possible — something which is very difficult experimentally. More likely, a real choice between the two models will first come from doing electroproduction off neutrons. From the first kind of model one expects in general sizable differences with respect to the proton, while in the second model the neutron and proton should be the same. Both of these experiments will be done within the next year at SLAC.

Looking back at the discussion of high energy electroproduction in the last electron-photon conference, I am amazed at how far we have come in exploring the $\nu - q^2$ plane experimentally. What was essentially a wilderness has now been rather completely mapped in a qualitative way, and in many cases we even know rather fine quantitative details of the landscape. One can only hope that by the time of the next conference there will be similar progress in understanding <u>why</u> the landscape in the $\nu - q^2$ plane has the particular form which has been so beautifully mapped out experimentally in the past two years.

## References


1. C. E. Dick and J. W. Motz, Phys. Rev. 171, 75 (1968).

2. P. Bounin and G. R. Bishop, J. Phys. Radium 22, 555 (1961).

3. See, for example, the recent calculation for $Ca^{40}$ by E. J. Moniz, Stanford University preprint, 1969 (unpublished).

4. We use a metric where $P^2 = P_\mu P_\mu = -M_N^2$ and $q^2 > 0$ corresponds to a space-like four-vector $q_\mu$. The fine structure constant $\alpha = e^2/4\pi \approx 1/137$ and the weak coupling constant $G \approx 1.0 \times 10^{-5}/M_N^2$. In our kinematic discussion we neglect lepton masses.

5. S. D. Drell and J. D. Walecka, Ann. Phys. (N.Y.) 28, 18 (1964).

6. L. N. Hand, Phys. Rev. 129, 1834 (1963).

7. For a discussion of the kinematics and the relations between the various amplitudes and cross sections see F. J. Gilman, Phys. Rev. 167, 1365 (1968).

8. E. D. Bloom et al., paper no. 99, contributed to this symposium; D. O. Caldwell et al., paper no. 33 contributed to this symposium; H. Meyer et al., paper no. 22 contributed to this symposium; J. Ballam et al., paper no. 8 contributed to this symposium; and J. Ballam et al., Phys. Rev. Letters 21, 1541 (1968).

9. E. D. Bloom et al., SLAC-PUB-642 and paper no. 98 contributed to this symposium.

10. For some of the previous large angle data see W. Albrecht et al., paper no. 20 contributed to this symposium, and references therein. Also see the discussion of the inelastic muon data in the invited talk by W. Toner, these proceedings.

11. See R. Taylor, these proceedings; SLAC Group A, private communication; W. Albrecht et al., paper no. 70 contributed to this symposium.

12. The behavior of $\sigma_S$ reminds one of the experimental situation for $\left[G_{En}(q^2)\right]^2$ (see J. Rutherglen, these proceedings) which must be zero at $q^2 = 0$, has a definite positive slope with respect to $q^2$ at $q^2 = 0$, but which is small and consistent within errors with zero at values of $q^2$ of a few GeV$^2$.

13. See J. D. Bjorken, "Current Algebra at Small Distances", Varenna School Lectures, Course XLI, Varenna, Italy (1967), where quarks are the point-like constituents.

14. R. P. Feynman (unpublished). In his development of the model, Feynman has coined the name "partons" for the constituent parts of the proton.

15. We follow rather closely here the discussion of J. D. Bjorken and E. A. Paschos, SLAC-PUB-572, 1969 (unpublished).

16. J. D. Bjorken, Phys. Rev. 179, 1547 (1969).

17. The first sum rule is essentially that proposed by K. Gottfried, Phys. Rev. Letters 18, 1174 (1967).

18. M. Breidenbach et al., SLAC-PUB-650, and paper no. 101 contributed to this symposium.

19. Note that if the ratio R is greater than zero, the value of $\nu W_2$ calculated from $d^2\sigma/d\Omega' dE'$ always increases compared to the value of $\nu W_2$ calculated assuming R = 0.

20. The author thanks Professor H. Harari for this remark.

21. If we drop the assumption of a symmetric momentum distribution then the value of $\int_0^1 F(x)dx$ can be changed rather drastically. See in this connection the work of S. D. Drell, D. J. Levy and T. M. Yan, reference 29.

22. The first work in this direction which the author knows of is that by Harari: see H. Harari, Phys. Rev. Letters 22, 1078 (1969). See also the discussion

of H. Abarbanel, M. L. Goldberger and S. B. Treiman, reference 30, and the discussion in section 5 of this talk. A particular type of diffraction model is also treated by R. W. Griffith, Argonne National Laboratory preprints, 1969 (unpublished).

23. See H. Harari, Phys. Rev. Letters 20, 1395 (1968); P. Freund, Phys. Rev. Letters 21, 235 (1968); F. J. Gilman, H. Harari, and Y. Zarmi, Phys. Rev. Letters 21, 323 (1968).

24. This can also be seen from the fact that in Regge language $\nu W_2 \to \nu^{\alpha(0)-1}$ and $W_1 \to \nu^{\alpha(0)}$ as $\nu \to \infty$ at fixed $q^2$, and $\alpha_p(0) = 1$.

25. Note that Eq. (17) tells us again that in the "flat" part of the "universal curve" the cross section is falling off slowly with respect to $q^2$, roughly like $1/q^2$, as noted in the description of the data in section 2.

26. H. Harari, private communication.

27. The first attempts in this direction, to the author's knowledge, were made by S. Berman and W. Schmidt (unpublished).

28. J. J. Sakurai, Phys. Rev. Letters 22, 981 (1969); C. F. Cho, G. J. Gounaris, and J. J. Sakurai, University of Chicago preprint, 1969 (unpublished). See also Y. S. Tsai, SLAC-PUB-600, 1969 (unpublished); J. D. Sullivan, University of Illinois preprint, 1969 (unpublished); and G. A. Piketty and L. Stodolsky in Proceedings of the Topical Conference on Weak Interactions, CERN, Geneva, 1969, (CERN 69-7) p. 75.

29. S. D. Drell, D. J. Levy, and T. M. Yan, Phys. Rev. Letters 22, 744 (1969) and S. D. Drell, D. J. Levy and T. M. Yan, SLAC-PUB-606, 1969 (unpublished).

30. H. Abarbanel, M. L. Goldberger, and S. B. Treiman, Phys. Rev. Letters 22, 500 (1969).

31. Also see the detailed study of G. Altarelli and H. Rubinstein, paper no. 19 contributed to this symposium.

32. H. Cheng and T. T. Wu, Phys. Rev. Letters 22, 666 (1969) and Phys. Rev., to be published.

33. S. J. Chang and S. K. Ma, Phys. Rev. Letters 22, 1334 (1969); H. Abarbanel and C. Itzykson, Phys. Rev. Letters 23, 53 (1969).

34. H. Cheng and T. T. Wu, Phys. Rev. Letters 22, 1409 (1969).

35. See, for example, H. Fraas and D. Schildknecht, paper no. 44 contributed to this symposium; M. J. Creutz, SLAC-PUB-610, 1969 (unpublished); S. D. Drell, D. J. Levy and T. M. Yan, reference 29 and to be published.

36. For some recent work on this subject see D. J. Gross and C. H. Llewellen Smith, CERN preprint, 1969 (unpublished); S. D. Drell, D. J. Levy and T. M. Yan, reference 29; J. D. Bjorken and E. A. Paschos, to be published.

37. I. Budagov et al., CERN preprint, 1969 (unpublished).

38. See, for example, J. Cornwall and R. Norton, Phys. Rev. 177, 2584 (1969); J. D. Bjorken, Phys. Rev. 163, 1767 (1967) and reference 16; C. Callan and D. Gross, Phys. Rev. Letters 21, 311 (1968); H. Burkhardt and W. N. Cottingham, University of Birmingham preprint, 1969 (unpublished).

39. C. Callan and D. Gross, Phys. Rev. Letters 22, 156 (1969).

40. S. L. Adler and W. K. Tung, Phys. Rev. Letters 22, 978 (1969).

41. R. Jackiw and G. Preparata, Phys. Rev. Letters 22, 975 (1969).

42. J. D. Bjorken, Phys. Rev. Letters 16, 408 (1966).

43. S. L. Adler, Phys. Rev. 143, 1144 (1966).

44. This is a particular case of a rather general feature of the diffraction or Pomeron model. If such a model is correct then the usual current algebra

sum rules decouple, in some sense, from the experiments on inelastic electron and neutrino scattering. In other words, if such a model is correct, the inelastic scattering has to do with the quantum numbers of the vacuum and not the internal quantum numbers of the target hadron, which are relevant to the current algebra sum rules.

45. See M. Bander, Weizmann Institute preprints, 1969 (unpublished); R. C. Brower and M. B. Halpern, Berkeley preprint, 1969 (unpublished); R. C. Brower and J. H. Weis, Berkeley preprints, 1969 (unpublished).

46. In the "explicit solution" given above, at least 0.13 out of the 0.34 at the peak of the $\nu W_2$ curve must be non-diffractive and vanish as $\nu \to \infty$ at fixed $q^2$.

47. W. N. Cottingham, Ann. of Phys. (N.Y.) 25, 424 (1963).

48. H. Harari, Phys. Rev. Letters 17, 1303 (196 ).

49. M. Elitzur and H. Harari, Weizmann Institute preprint, 1969 (unpublished); R. Chanda, University of Maryland preprint, 1969 (unpublished); D. J. Gross and H. Pagels, Phys. Rev. 172, 1381 (1968).

50. M. J. Creutz, S. D. Drell and E. A. Paschos, Phys. Rev. 178, 2300 (1969).

51. F. J. Gilman, unpublished; M. Damashek and F. J. Gilman, to be published.

52. The precise magnitude of such a real constant of course depends on the measured cross sections as well as on the Regge pole form for the amplitudes at high energies, whose parameters are fixed by a fit to the high energy data. Conversations at SLAC with M. Creutz and at the conference, particularly with Dr. M. Wong from DESY, indicate that perhaps the errors on the measured total cross sections (particularly the differences between the measurements of different groups) are large enough and the Regge parameters free enough that one can find an acceptable Regge parametrization of the high

energy data which makes the extra real constant go away, i.e., be consistent with zero.

53. If the extra real constant does have the magnitude of the Thomson limit (so that it is associated with the nucleon Born term in Compton scattering), it should be noted that the amplitude $t_1(\nu,q^2)$ is <u>not</u> the one which obeys a low energy theorem at $q^2 = 0$ (the Born contribution to $t_1(\nu,q^2)$ vanishes at $q^2 = 0$). Thus we might not expect a fixed pole in $t_1(\nu,q^2)$ at $q^2 = 0$ if the fixed pole is associated with the Born term. Away from $q^2 = 0$ it appears anything could happen.

## Figure Captions

Figure 1 - Inelastic electron scattering from Aluminum and Gold atoms[1]. The incident energy is 400 keV and the final electron energy is directly proportional to the channel number.

Figure 2 - Inelastic scattering of 194 MeV electrons at $135^{\circ}$ form the $C^{12}$ nucleus[2].

Figure 3 - Kinematics of inelastic electron-nucleon scattering.

Figure 4 - The total photoabsorption cross section, $\sigma_T(\gamma p)$ measured in recent experiments[8].

Figure 5 - A kinematic map of the $\nu - q^2$ plane.

Figure 6 - Fixed $\theta$ lines in the $\nu - q^2$ plane along which data was taken in the recent SLAC experiments.

Figure 7 - The spectrum[9] at $\theta = 6^{\circ}$, E = 10.0 GeV (a) before and (b) after radiative corrections. The ratio of the radiatively corrected to the uncorrected cross section is shown in (c).

Figure 8 - Radiatively corrected spectra[9] at increasing energies and angles: (a) $\theta = 6^{\circ}$, E = 7 GeV; (b) $\theta = 6^{\circ}$, E = 16 GeV; (c) $\theta = 10^{\circ}$, E = 17.7 GeV.

Figure 9 - Kinematics of inelastic electron scattering in the parton model[15].

Figure 10 - Plots[18] of $\nu W_2$ versus $\omega = 2M_N\nu/q^2$ for (a) the $\theta = 6^{\circ}$, E = 7 GeV data if R = 0 or $\infty$; (b) the $\theta = 6^{\circ}$ data, except for the E = 7 GeV spectrum, for R = $\infty$; (c) the $\theta = 6^{\circ}$ data, except for the E = 7 GeV spectrum, for R = 0.

Figure 11 - Plots[18] of $\nu W_2$ versus $\omega = 2M_N\nu/q^2$ for (a) the $\theta = 10^{\circ}$ data for R = $\infty$; (b) the $\theta = 10^{\circ}$ data for R = 0.

Figure 12 - Plot of $\nu W$ from both the $\theta = 6^{\circ}$ and $10^{\circ}$ data versus $x = q^2/2M\nu$ assuming $R = 0$ and taking data points with $q^2 \geq 1$ GeV$^2$ only.

Figure 13 - $\nu W_2$ versus $2M_N\nu/q^2$ from the $\theta = 6^{\circ}$ and $10^{\circ}$ data assuming $R = 0$ and taking data points with $W \geq 2.0$ GeV only.

Figure 14 - $W_1$ versus $2M_N\nu/q^2$ from the $\theta = 6^{\circ}$ and $10^{\circ}$ data assuming $R = 0$ and taking data points with $W \geq 2.0$ GeV only.

Figure 15 - $F(x) = \nu W_2$ versus $x = q^2/2M_N\nu$ for two "extreme" cases of the parton model. The open circles indicate roughly the position of the "universal curve" indicated by the $\theta = 6^{\circ}$ and $10^{\circ}$ data if $R = 0$.

Figure 16 - $\nu W_2$ plotted versus $\nu$ for the $\theta = 6^{\circ}$ and $10^{\circ}$ data points with $q^2 = 0.75 \pm 0.075$ GeV$^2$. Note that the zero point of the scale for $\nu W_2$ lies off the figure.

Figure 17 - $\nu W_2$ plotted versus $\nu$ for the $\theta = 6^{\circ}$ and $10^{\circ}$ data points with $q^2 = 1.0 \pm 0.1$ GeV$^2$.

Figure 18 - $\nu W_2$ plotted versus $\nu$ for the $\theta = 6^{\circ}$ and $10^{\circ}$ data points with $q^2 = 2.0 \pm 0.2$ GeV$^2$.

Figure 19 - Kinematics of electron-positron annihilation into a proton plus "anything".

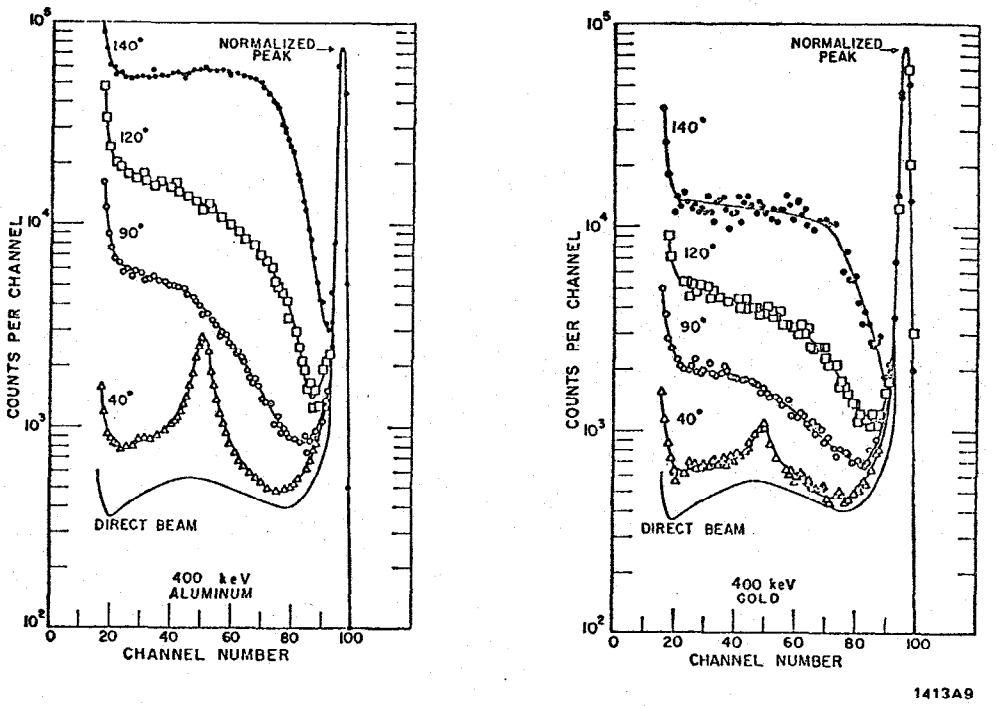
COUNTS PER CHANNEL
CHANNEL NUMBER
NORMALIZED PEAK
140°
120°
90°
40°
DIRECT BEAM
400 keV
ALUMINUM
400 keV
GOLD
1413A9

Fig. 1

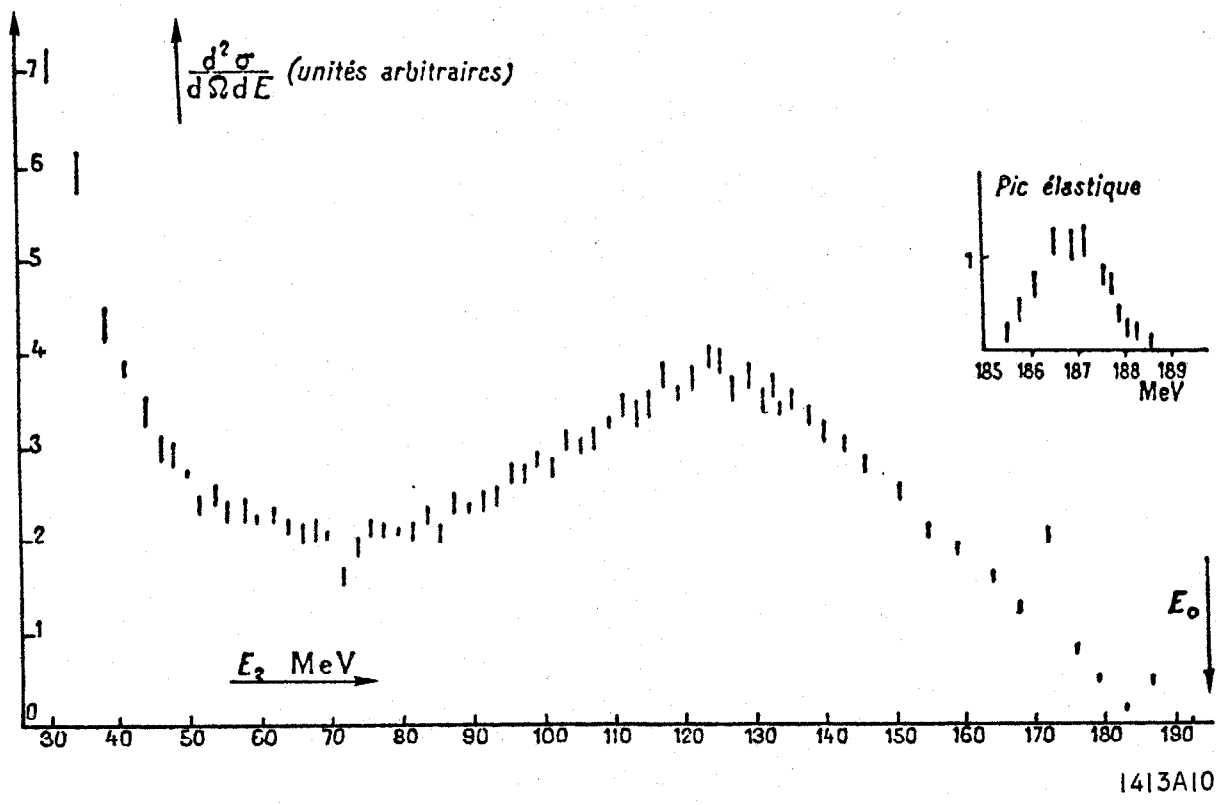
$\frac{d^2\sigma}{d\Omega dE}$ (unités arbitraires)
Pic élastique
185 186 187 188 189
MeV
$E_x$ MeV
$E_o$
0 1 2 3 4 5 6 7
30 40 50 60 70 80 90 100 110 120 130 140 150 160 170 180 190
1413A10

Fig. 2

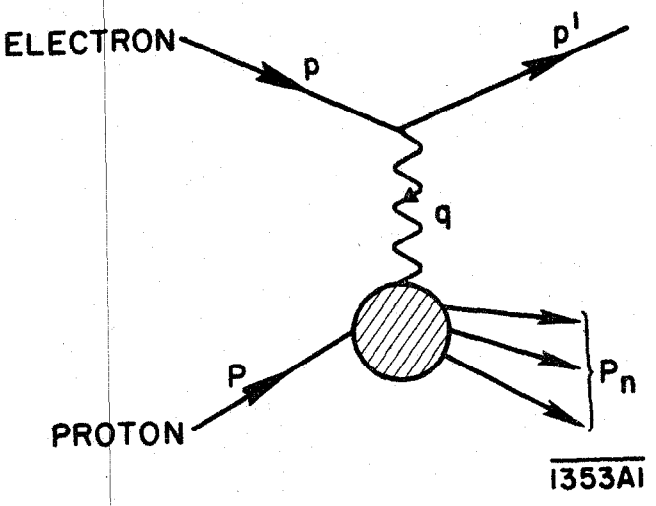


Fig. 3

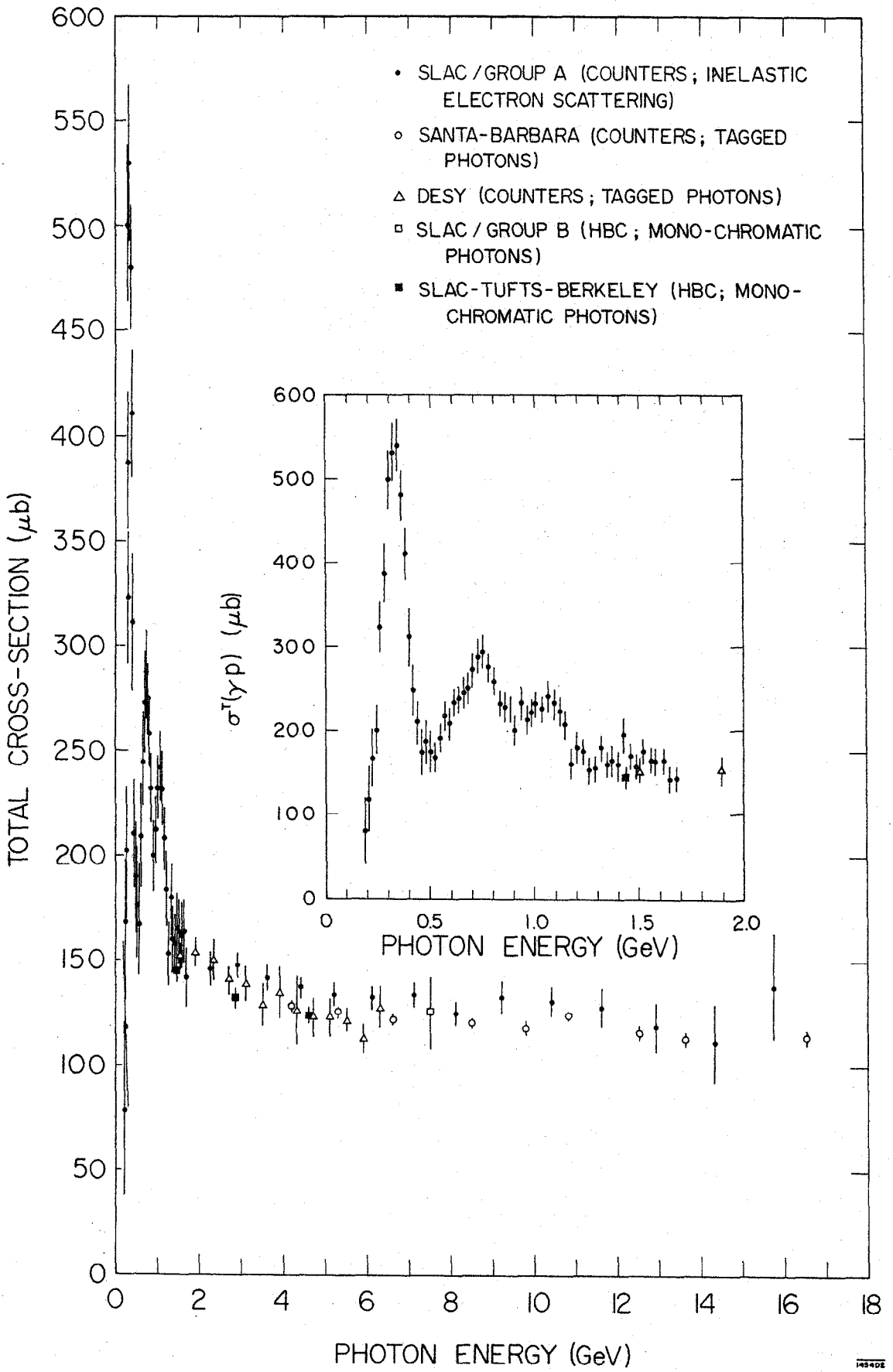
• SLAC / GROUP A (COUNTERS; INELASTIC ELECTRON SCATTERING)
○ SANTA-BARBARA (COUNTERS; TAGGED PHOTONS)
△ DESY (COUNTERS; TAGGED PHOTONS)
□ SLAC / GROUP B (HBC; MONO-CHROMATIC PHOTONS)
■ SLAC-TUFTS-BERKELEY (HBC; MONO-CHROMATIC PHOTONS)
TOTAL CROSS-SECTION (μb)
PHOTON ENERGY (GeV)
σ^T(γp) (μb)
PHOTON ENERGY (GeV)

Fig. 4

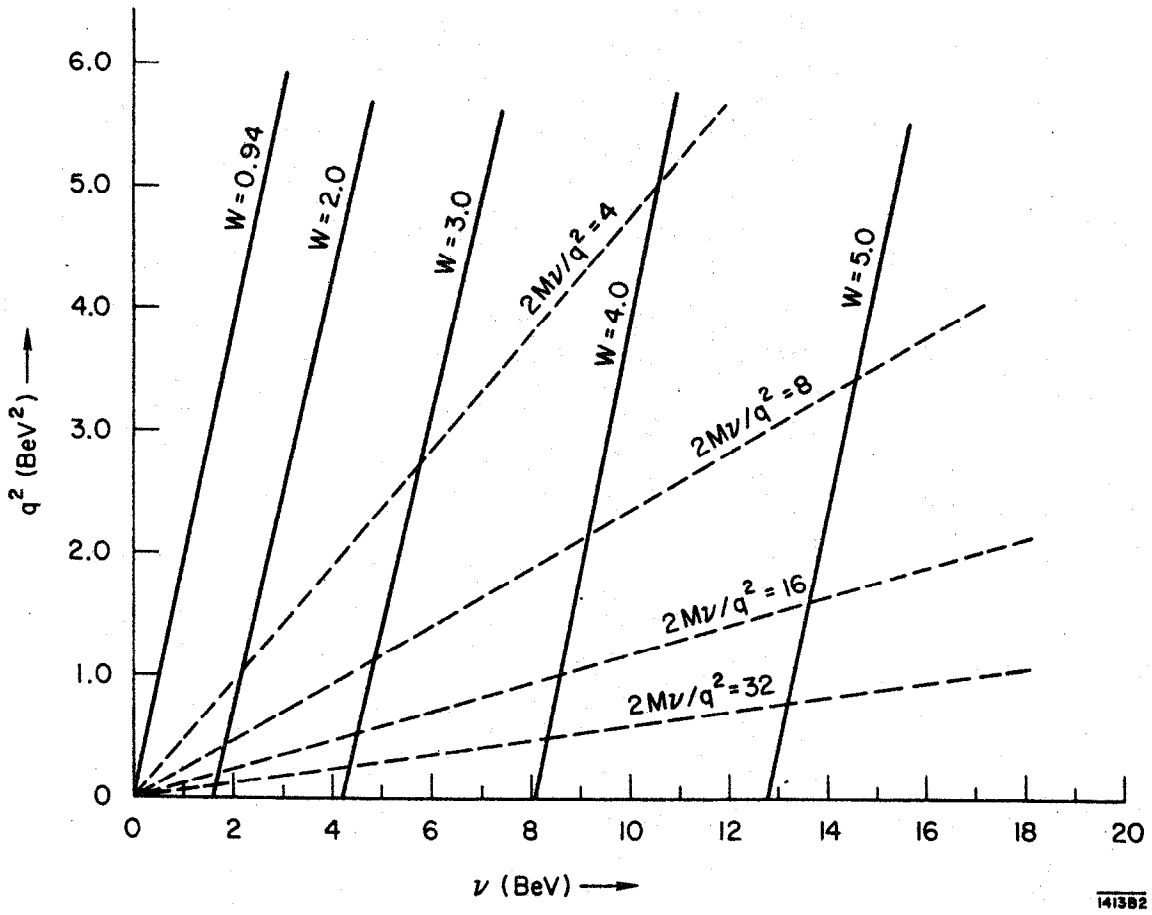
6.0
5.0
4.0
3.0
2.0
1.0
0
$q^2$ (BeV$^2$) ⟶
0
2
4
6
8
10
12
14
16
18
20
$\nu$ (BeV) ⟶
W=0.94
W=2.0
W=3.0
W=4.0
W=5.0
$2M\nu/q^2=4$
$2M\nu/q^2=8$
$2M\nu/q^2=16$
$2M\nu/q^2=32$
141382

Fig. 5

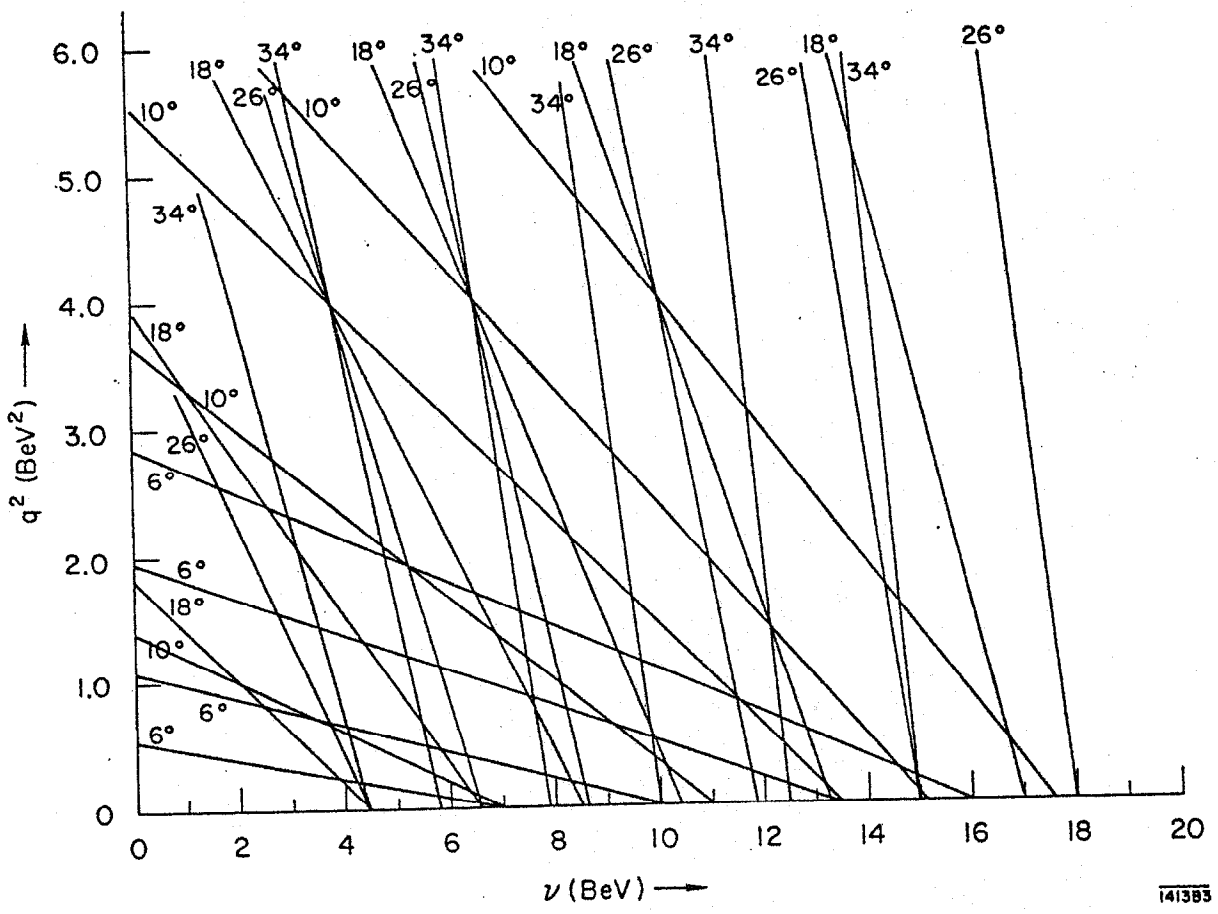


Fig. 6

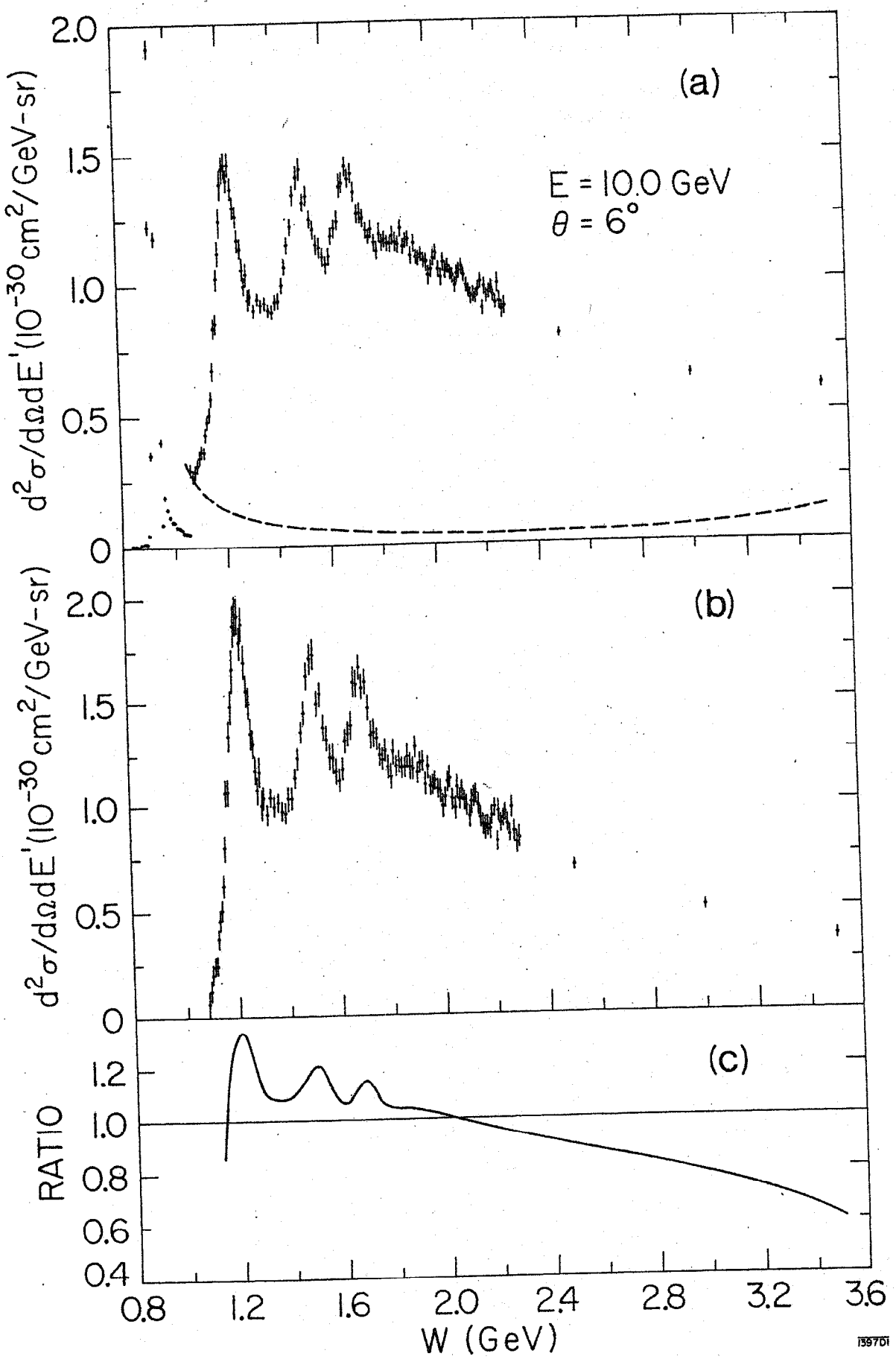
(a)
E = 10.0 GeV
θ = 6°
d²σ/dΩdE' (10⁻³⁰ cm²/GeV-sr)
(b)
d²σ/dΩdE' (10⁻³⁰ cm²/GeV-sr)
(c)
RATIO
W (GeV)
139701

Fig. 7

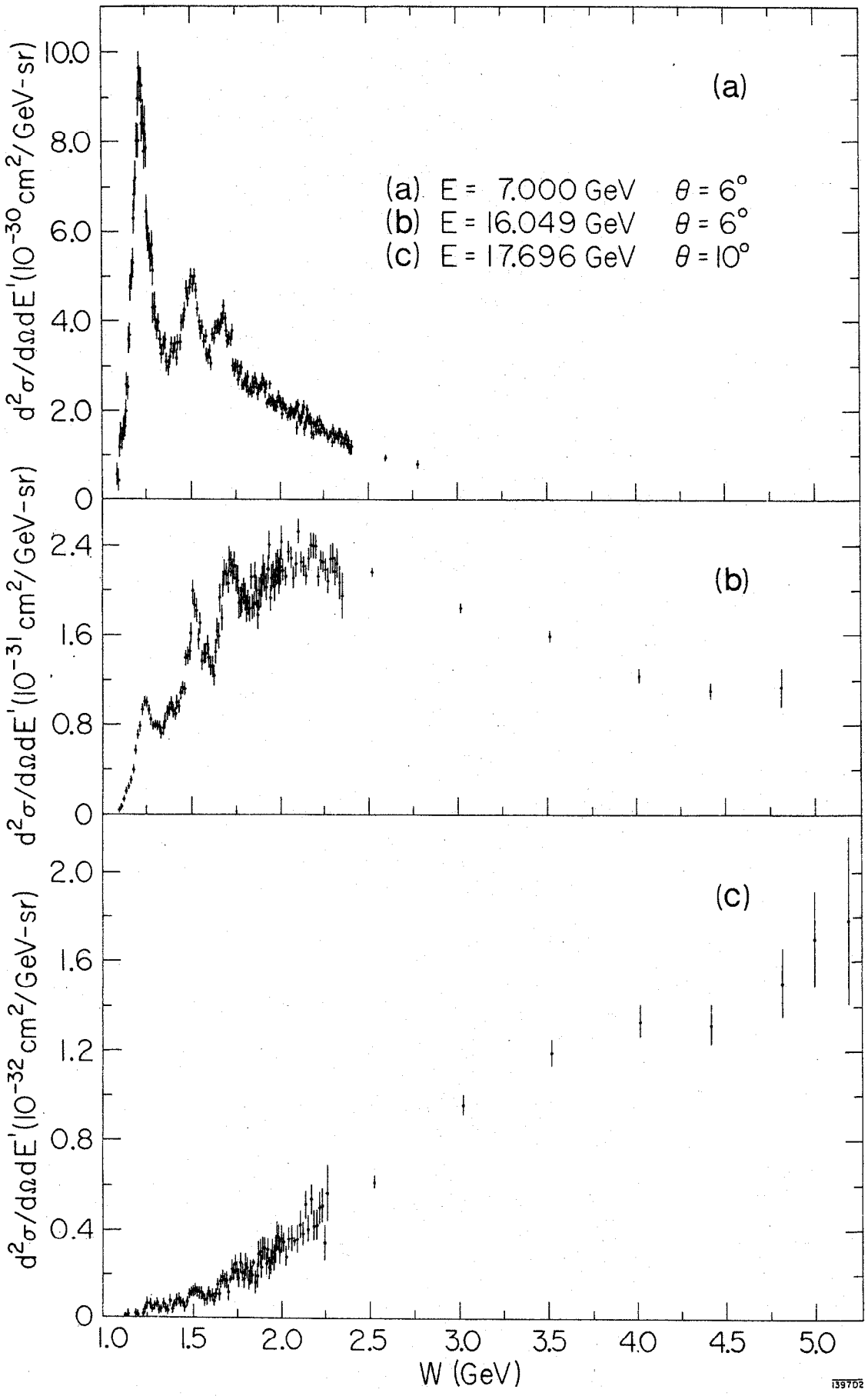
(a)
(a) E = 7.000 GeV θ = 6°
(b) E = 16.049 GeV θ = 6°
(c) E = 17.696 GeV θ = 10°
(b)
(c)
d²σ/dΩdE'(10⁻³⁰ cm²/GeV-sr)
d²σ/dΩdE'(10⁻³¹ cm²/GeV-sr)
d²σ/dΩdE'(10⁻³² cm²/GeV-sr)
W (GeV)
139702

Fig. 8

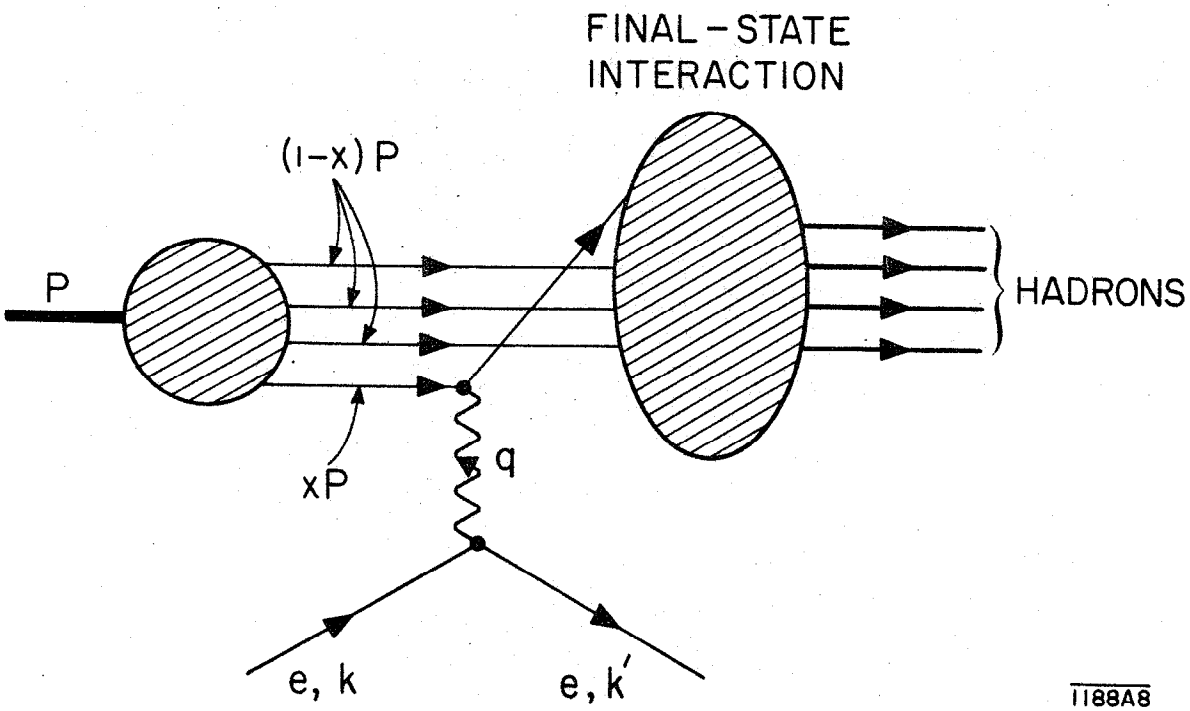


Fig. 9

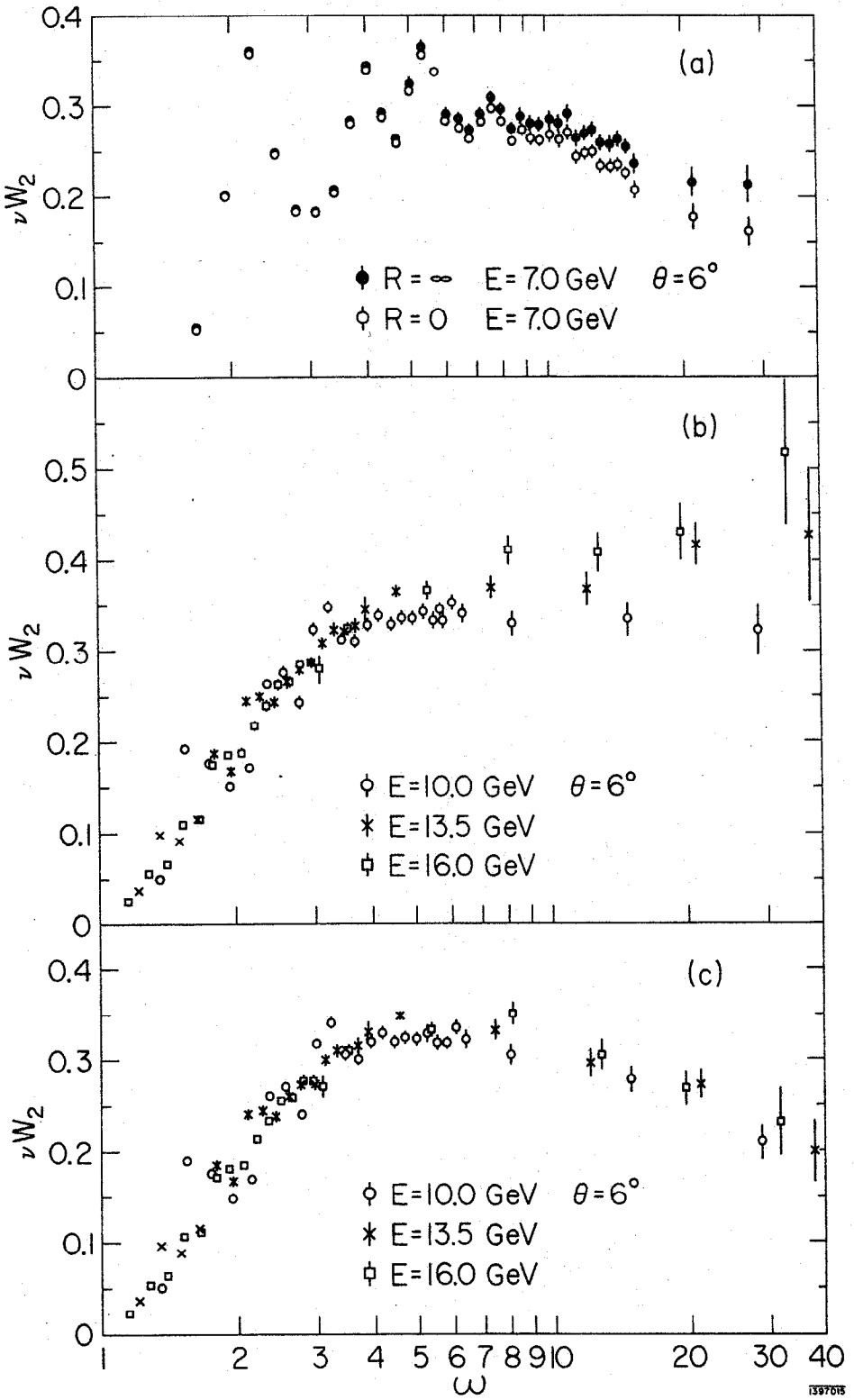
(a)
R = ∞ E = 7.0 GeV θ = 6°
R = 0 E = 7.0 GeV
(b)
E = 10.0 GeV θ = 6°
E = 13.5 GeV
E = 16.0 GeV
(c)
E = 10.0 GeV θ = 6°
E = 13.5 GeV
E = 16.0 GeV
νW2
ω
0.4
0.3
0.2
0.1
0
0.5
1
2
3
4
5
6
7
8
9
10
20
30
40
139701S

Fig. 10

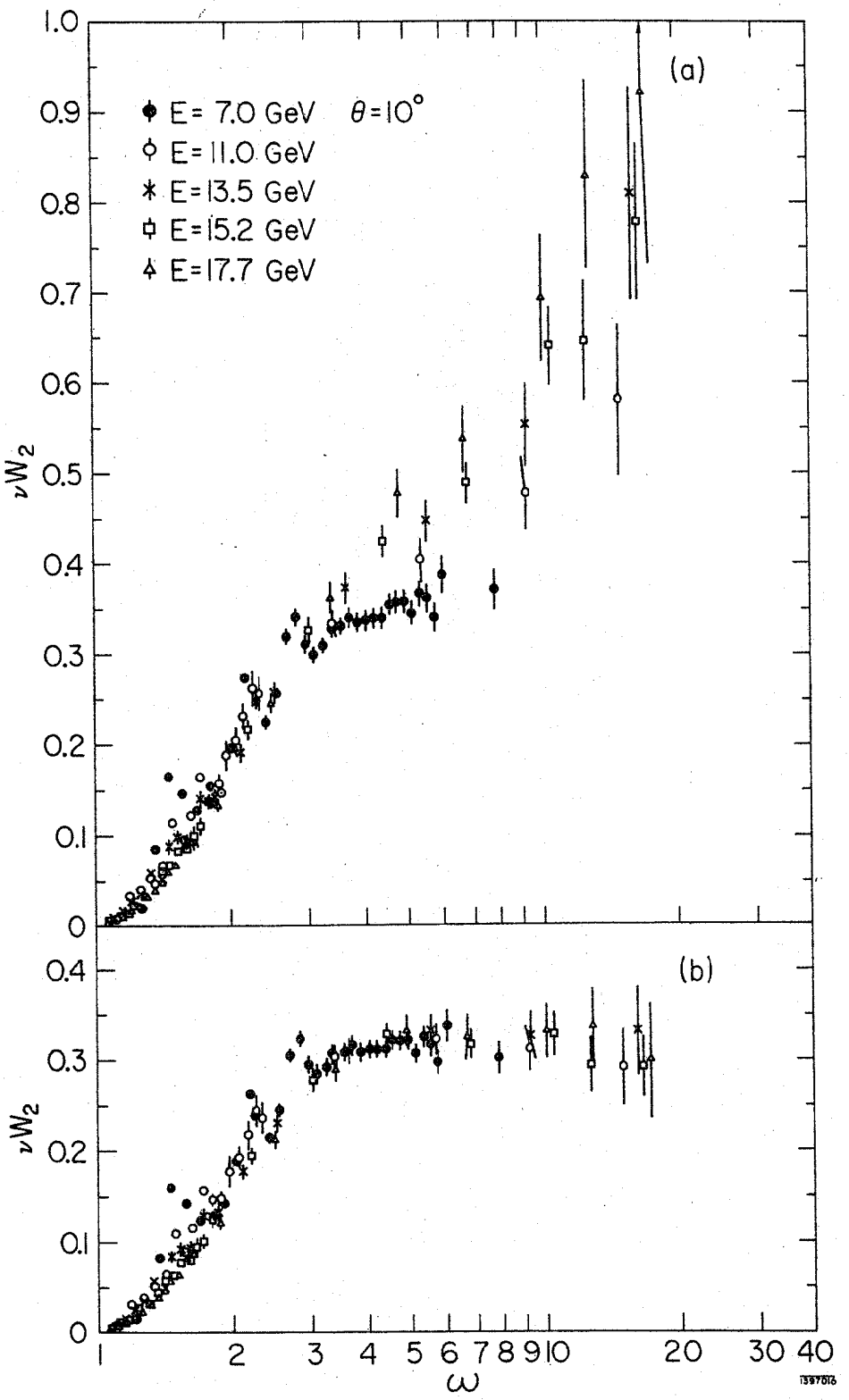


Fig. 11

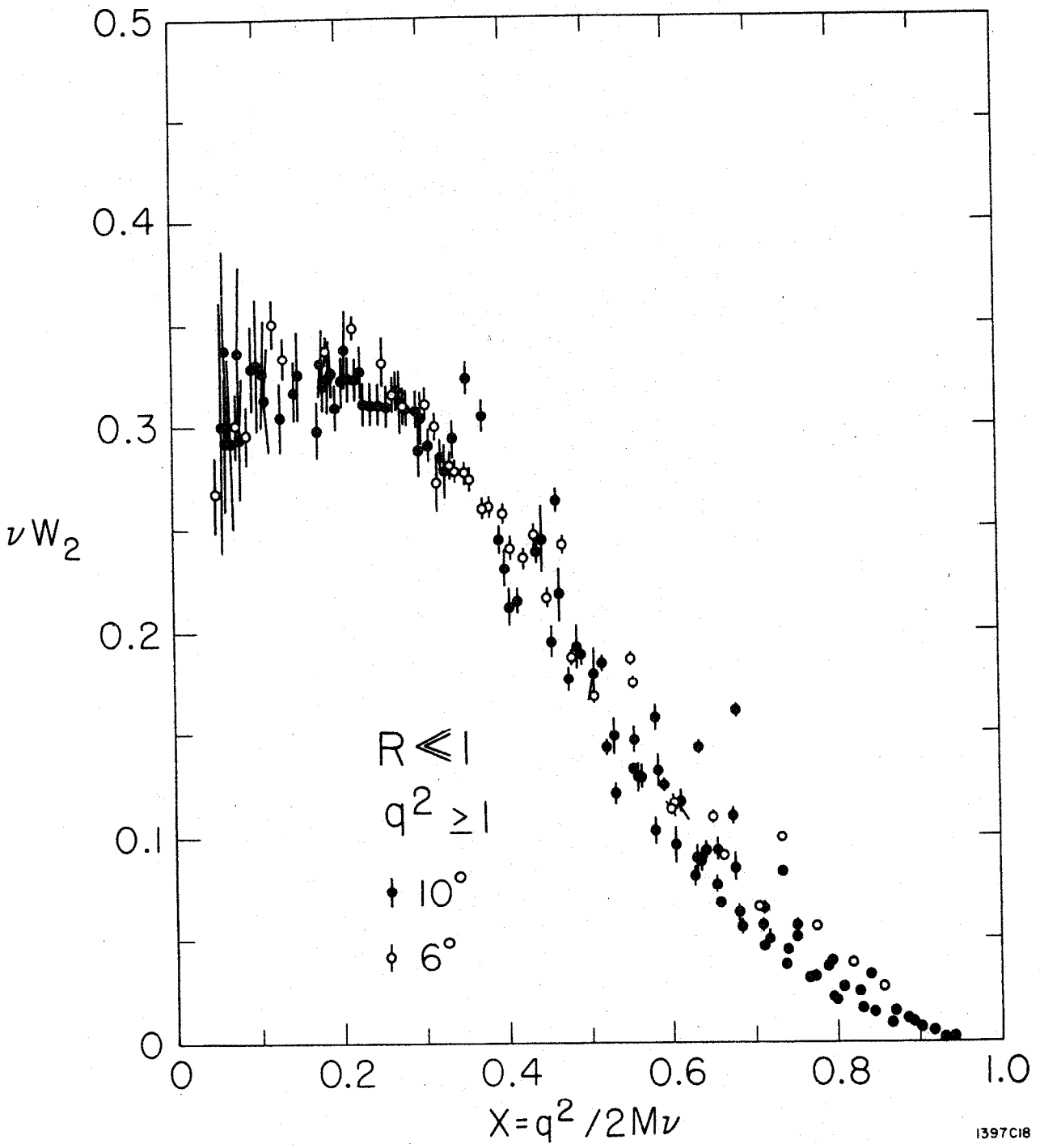
0.5
0.4
0.3
0.2
0.1
0
$\nu W_2$
$R \ll 1$
$q^2 \geq 1$
10°
6°
0
0.2
0.4
0.6
0.8
1.0
$X = q^2/2M\nu$
1397C18

Fig. 12

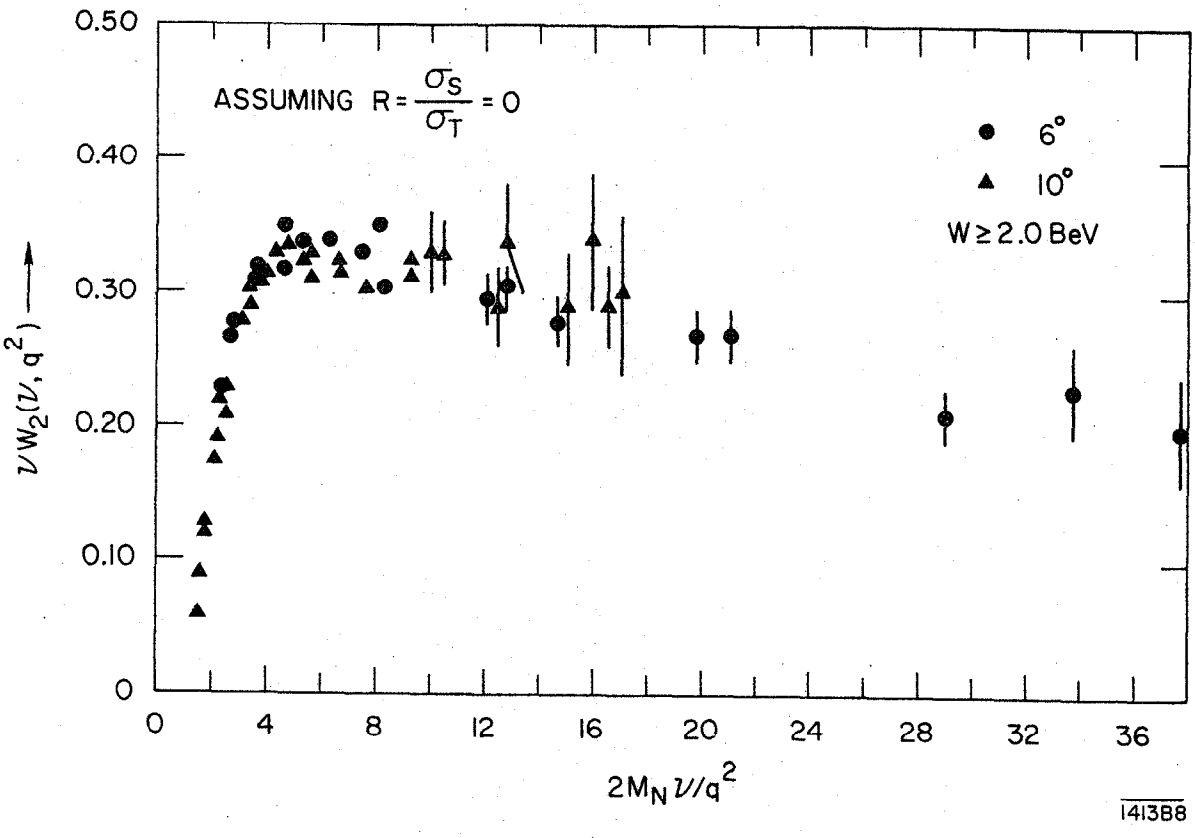
0.50
0.40
0.30
0.20
0.10
0
ASSUMING $R = \frac{\sigma_S}{\sigma_T} = 0$
6°
10°
W ≥ 2.0 BeV
$\nu W_2(\nu, q^2)$
0
4
8
12
16
20
24
28
32
36
$2M_N \nu/q^2$
141388

Fig. 13

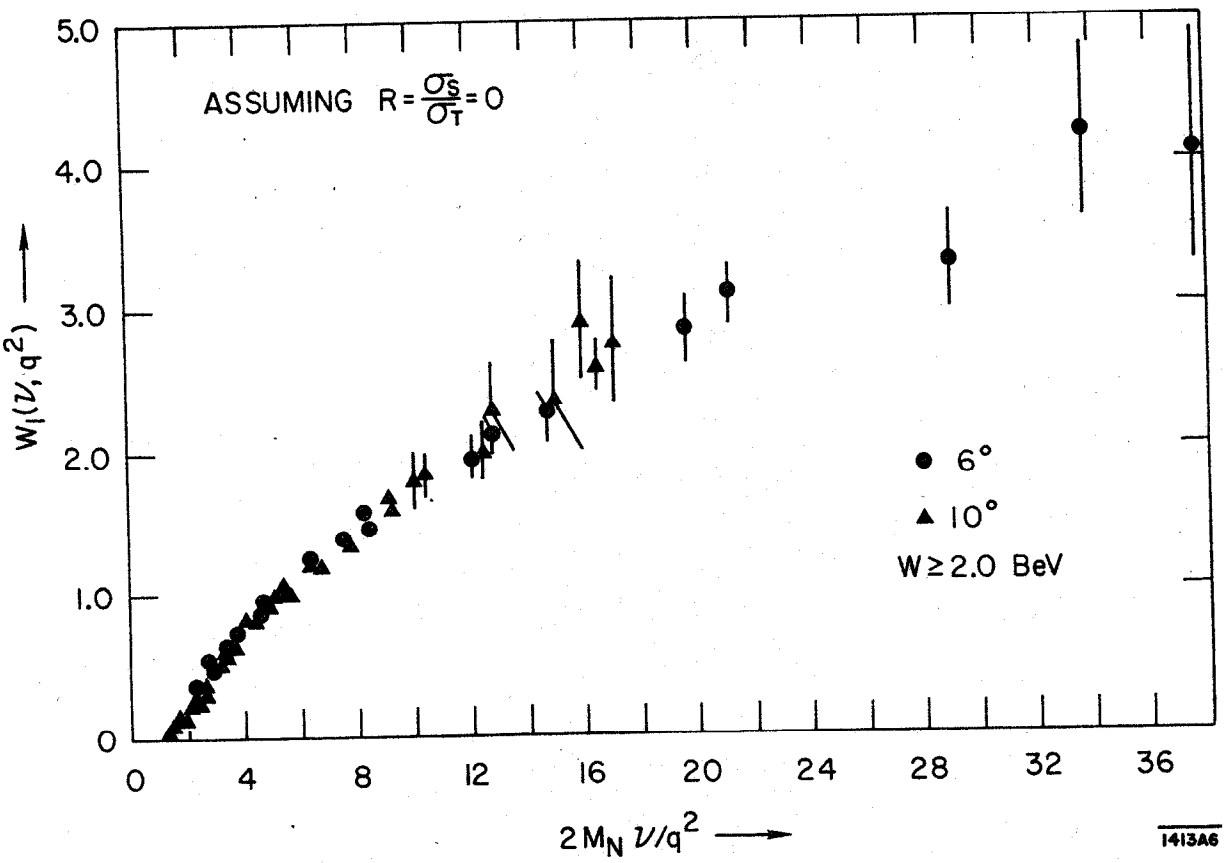
ASSUMING $R = \frac{\sigma_S}{\sigma_T} = 0$
$W_1(\nu, q^2)$
$2M_N \nu/q^2$
6°
10°
W ≥ 2.0 BeV
0
1.0
2.0
3.0
4.0
5.0
0
4
8
12
16
20
24
28
32
36
1413A6

Fig. 14

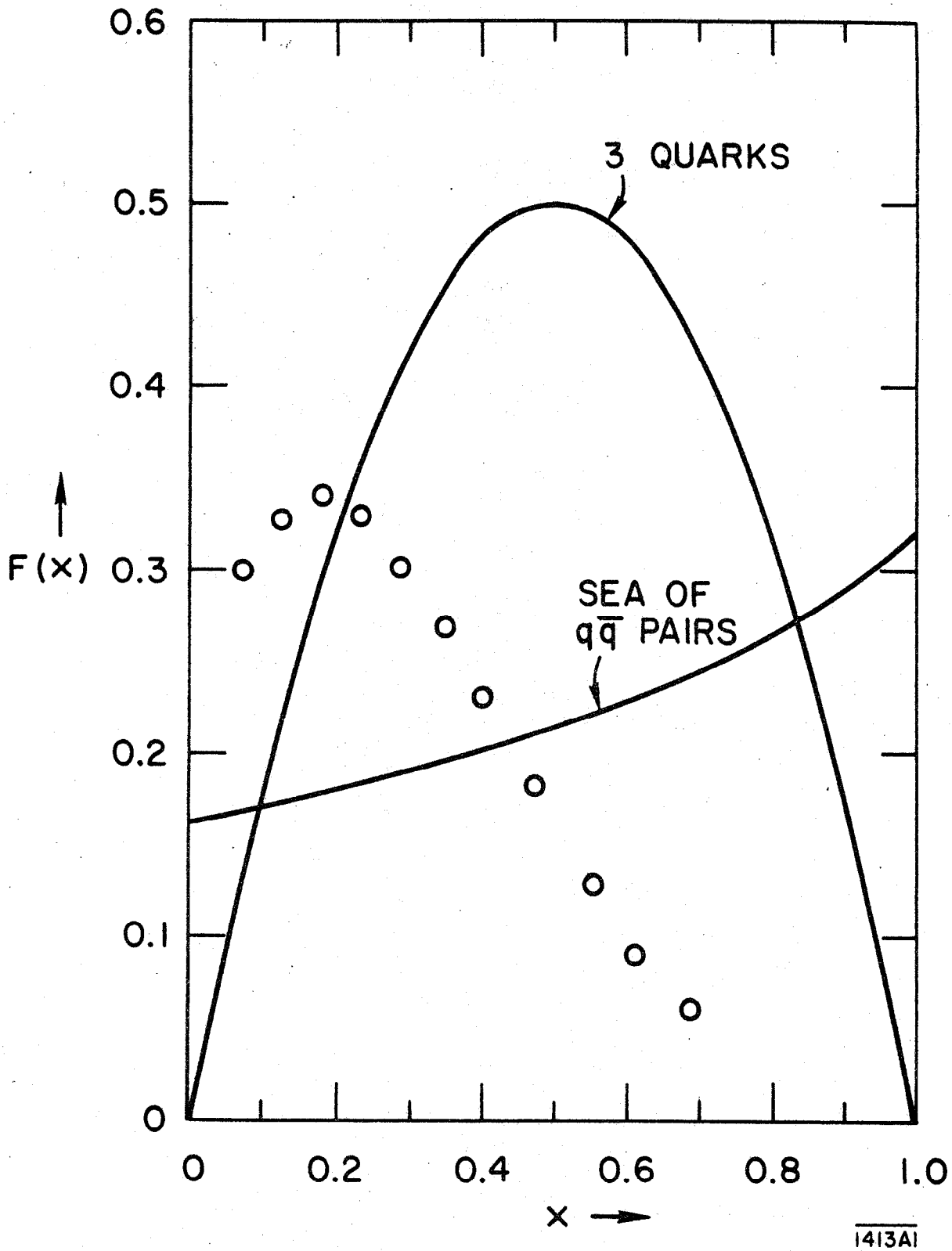
0.6
0.5
0.4
0.3
0.2
0.1
0
F(x)
3 QUARKS
SEA OF
$q\bar{q}$ PAIRS
0
0.2
0.4
0.6
0.8
1.0
x
1413A1

Fig. 15

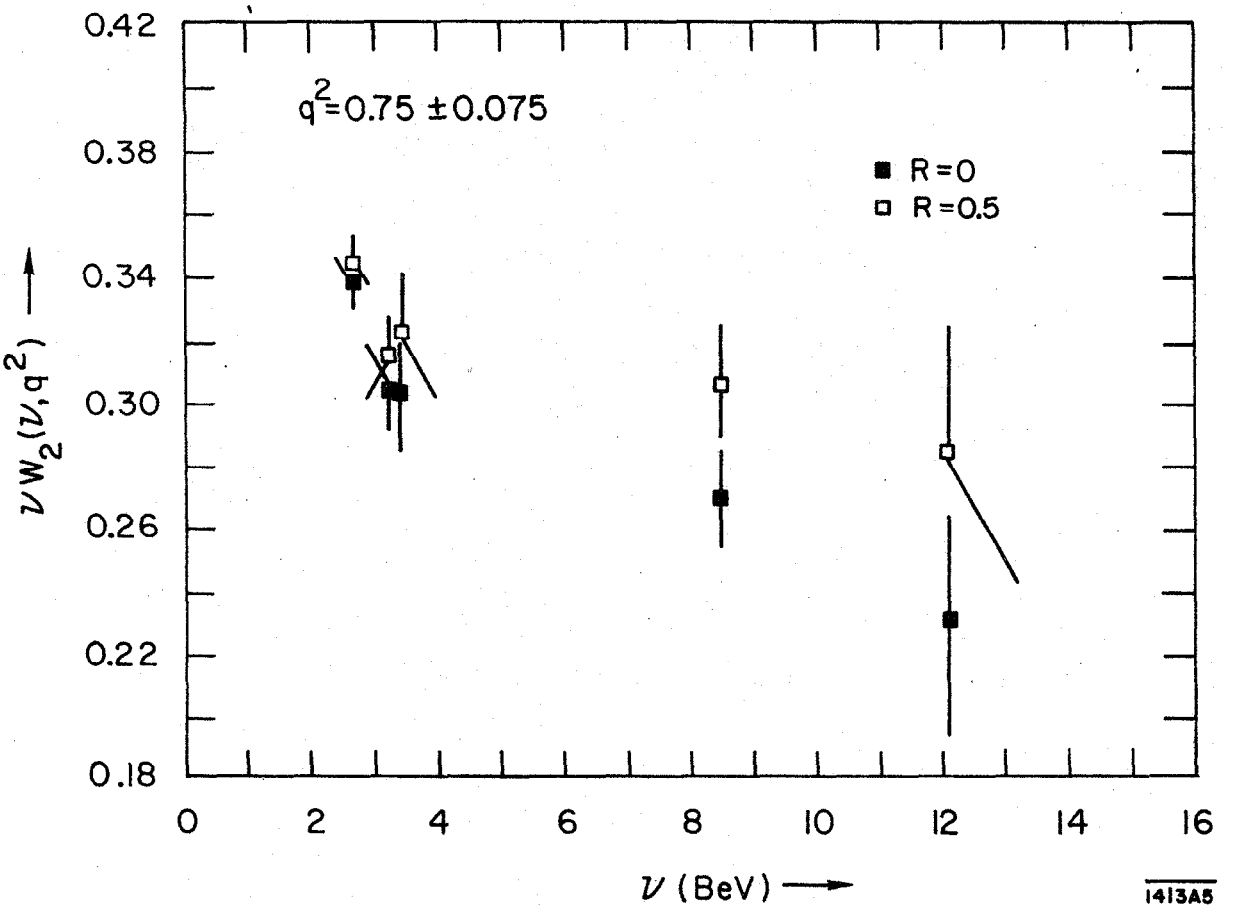
0.42
0.38
0.34
0.30
0.26
0.22
0.18
$q^2$=0.75 ±0.075
R=0
R=0.5
$\nu W_2(\nu, q^2)$
0
2
4
6
8
10
12
14
16
$\nu$ (BeV)
1413A5

Fig. 16

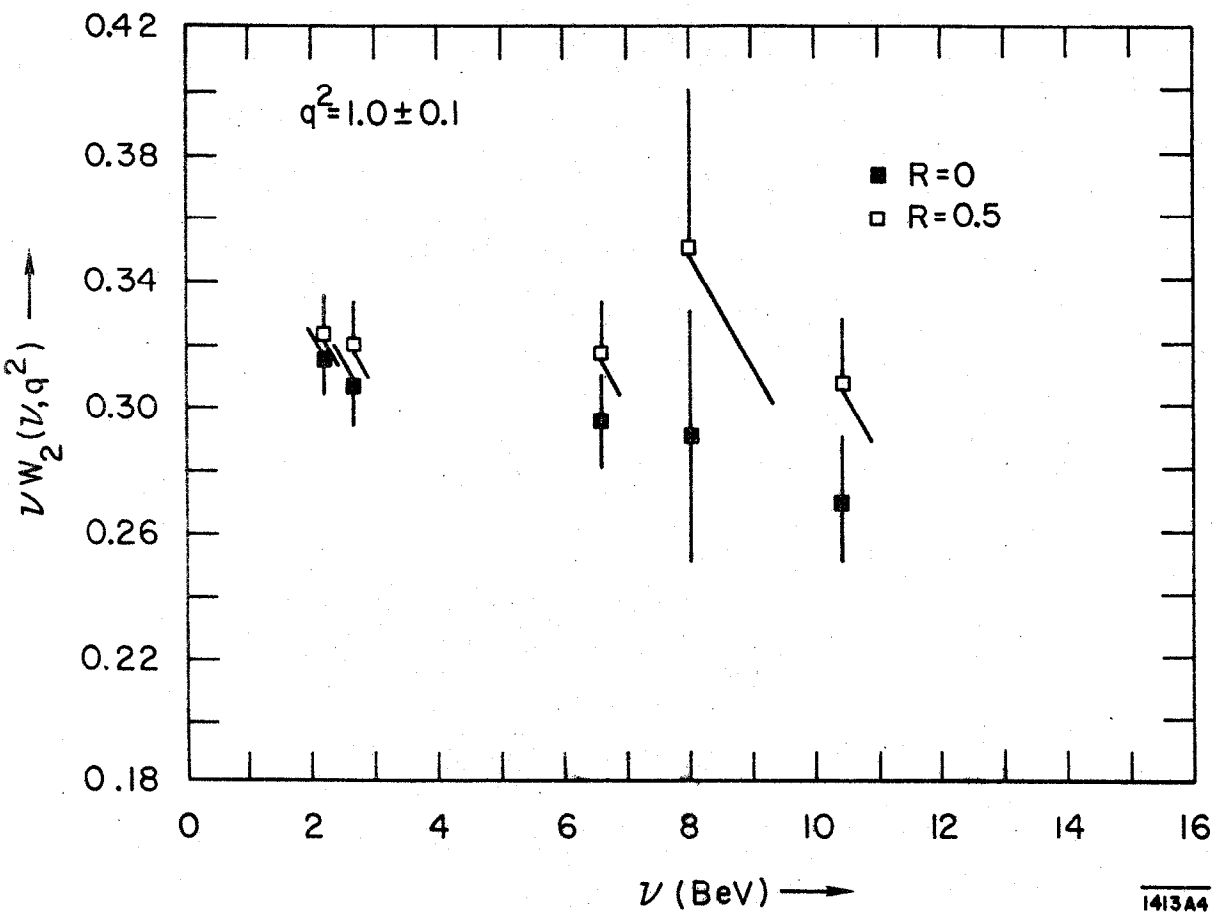
0.42
0.38
0.34
0.30
0.26
0.22
0.18
$q^2 = 1.0 \pm 0.1$
R=0
R=0.5
$\nu W_2(\nu, q^2)$
0
2
4
6
8
10
12
14
16
$\nu$ (BeV)
1413A4

Fig. 17

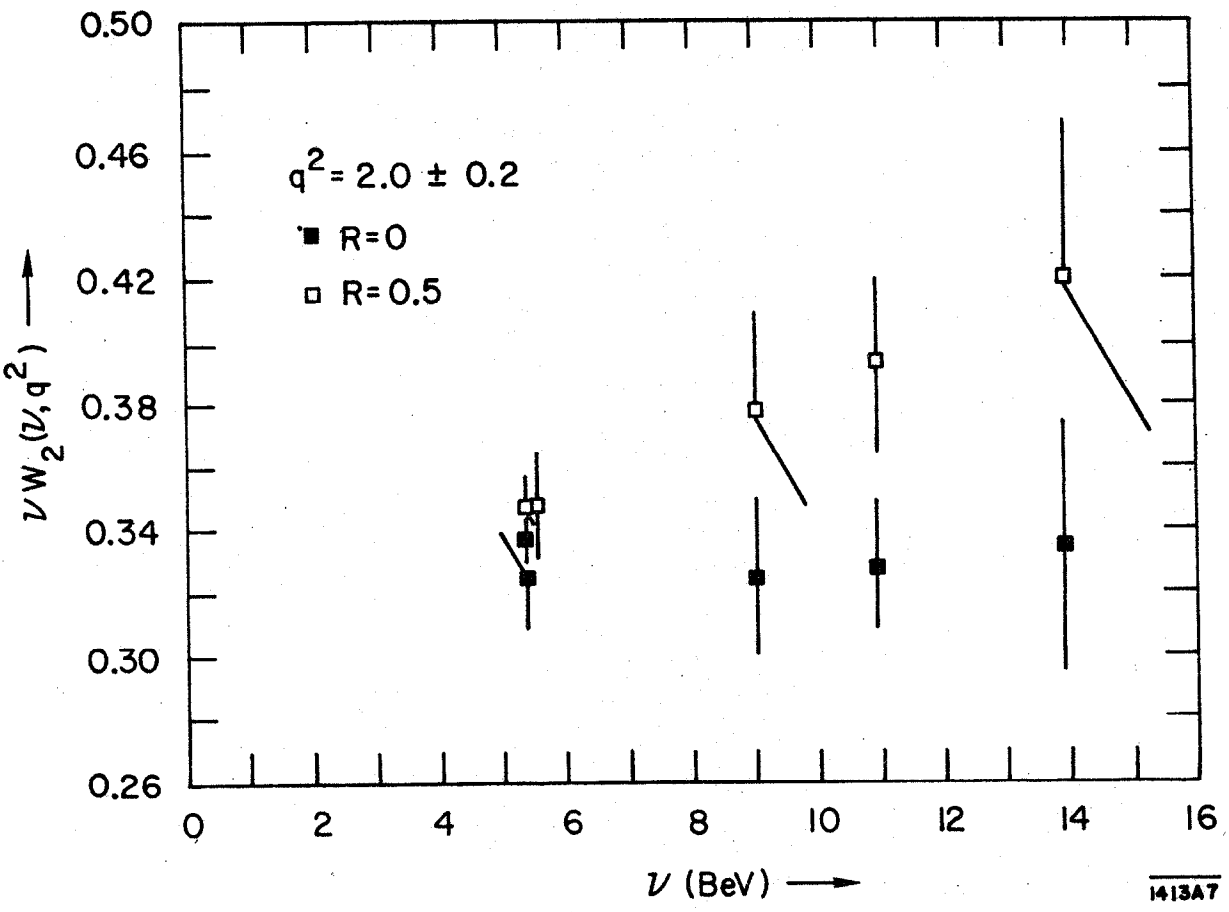
0.50
0.46
0.42
0.38
0.34
0.30
0.26
$\nu W_2(\nu, q^2)$
$q^2 = 2.0 \pm 0.2$
R=0
R=0.5
0
2
4
6
8
10
12
14
16
$\nu$ (BeV)
1413A7

Fig. 18

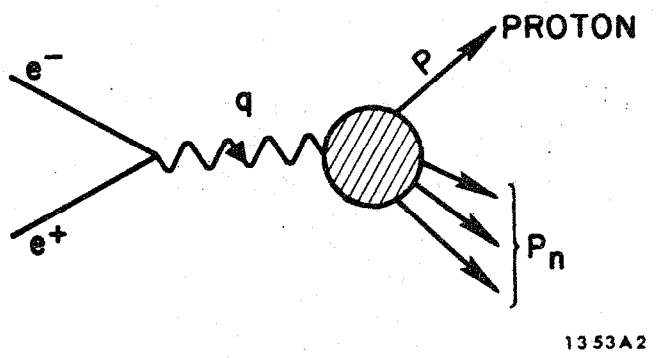


Fig. 19